mice suggests that other TLRs may be involved in IFN production by AcNPV. However, PECs from mice deficient in TLR3 and TLR7, which recognize dsRNA and single-stranded RNA, respectively, exhibited no reduction of IFN-α production upon infection with AcNPV (Fig. 1B). These results suggest that a novel cytoplasmic DNA-sensing mechanism other than TLR3, TLR7, and TLR9 signaling pathways might be involved in the production of type I IFN in PECs upon infection with AcNPV.

Although AcNPV contains a high level of unmethylated CpG DNA comparable to that found in the genomes of *E. coli* and HSV (1), the involvement of a TLR9/MyD88 signal pathway in the production of type I IFN by the AcNPV genome remains unclear. *E. coli* DNA and phosphorothioate-stabilized mCpG oligonucleotides (ODN1668) were capable of producing a large amount of IL-12 in PECs through a TLR9/MyD88-dependent pathway, whereas production of type I IFN was not induced by the ligands (Fig. 1C). Production of IL-12 and IFN-α in PECs transfected with the purified baculoviral DNA was impaired by knockout of the TLR9 or the MyD88 gene, whereas substantial amounts of IFN-β were still produced in PECs derived from MyD88- or TLR9-deficient mice (Fig. 1C). These results suggest that a TLR9/MyD88-independent DNA recognition pathway participates in the production of type I IFN in PECs in response to the AcNPV genome.

pDCs are known as master producers of type I IFN upon virus infection, and IFN production is largely dependent on the TLR signaling pathway (11). IFN-α production in pDCs derived from TLR9- or MyD88-deficient mice was severely impaired in response to AcNPV stimulation (Fig. 1D), suggesting that AcNPV induces IFN-α production in pDCs through a TLR9/MyD88-dependent pathway. Next, to examine the mechanisms of induction of type I IFN by AcNPV in vivo, AcNPV was intraperitoneally inoculated into wild-type and MyD88- or TLR9-deficient mice, and levels of IFN-α and IL-12 production in sera were determined. TLR9- or MyD88-deficient mice exhibited a level of serum IFN-α similar to that of wild-type mice upon infection with AcNPV, whereas IL-12 production in the deficient mice was severely impaired (Fig. 1E). These results suggest that non-pDCs participate in the production of type I IFN through a TLR9/MyD88-independent pathway in response to AcNPV in vivo, in contrast to the TLR9/MyD88-dependent production of proinflammatory cytokines. Collectively, these results indicate that both TLR-dependent and -independent pathways are involved in the production of type I IFN in immune cells, including PECs, $CD11c^+$ DCs, and pDCs, in response to AcNPV.

IRF7 plays a crucial role in the production of type I IFN by AcNPV in immune cells and in mice. Both IRF3 and IRF7 are required for the production of type I IFN through a classical pathway activated by viral infection (18, 41). Therefore, we examined the involvement of IRF3 and IRF7 in the production of type I IFN in response to AcNPV by using PECs and splenic $CD11c^+$ DCs derived from IRF3- and IRF7-deficient mice (Fig. 2A). IFN-α production in the IRF7-deficient PECs and splenic $CD11c^+$ DCs in response to AcNPV or VSV was impaired, whereas such production was still active in the IRF3-deficient immune cells. IFN-β production in PECs was impaired in the IRF3- or IRF7-deficient mice in response to AcNPV, although significant amounts of IFN-β were produced in the IRF3- or IRF7-deficient PECs upon infection with VSV. In contrast to the PECs, IRF3-deficient splenic $CD11c^+$ DCs produced a level of IFN-β comparable to that in the wild-type cells in response to AcNPV. In response to VSV infection, production of IFN-β in the deficient immune cells was less impaired. Although enhancement of IL-12 production in the IRF3-deficient PECs and splenic $CD11c^+$ DCs in response to AcNPV or VSV was observed, similar levels of IL-12 production were observed in the IRF7-deficient immune cells and in wild-type cells in response to AcNPV or VSV.

There is circumstantial evidence that IRF7 plays a role in the MyD88-dependent production of IFN-α by activating the TLR in pDCs (17, 25). Therefore, we next examined the IFN-α production in pDCs obtained from IRF7-deficient mice. Consistent with the previous observations, IFN-α production in response to AcNPV was completely abolished in the IRF7-deficient pDCs (Fig. 2B). Furthermore, production of IFN-α, but not that of IL-12 and IL-6, in response to AcNPV in IRF7-deficient mice was severely impaired (Fig. 2C). These results suggest that IRF7 plays a crucial role in the production of type I IFN upon infection with AcNPV in the immune cells and in vivo.

Involvement of the IFNR signaling pathway in the production of type I IFN by AcNPV. The many subtypes of IFN-α and IFN-β are released from infected cells and bind to a single IFNR, and receptor-mediated signal transduction induces the expression of numerous IFN-stimulated genes whose products interfere with viral replication. To determine the involvement of the IFNR-mediated signal transduction in the induction of the innate immune response by AcNPV infection, production of IFN-α, IFN-β, and IL-12 in PECs and splenic $CD11c^+$ DCs derived from IFNR-deficient mice after stimulation with AcNPV or poly(I:C) was examined. Production of IFN-α and IFN-β was significantly impaired by AcNPV or poly(I:C) in the IFNR-deficient PECs and splenic $CD11c^+$ DCs (Fig. 3A and B), whereas IL-12 production in the deficient immune cells was comparable to that in the wild-type cells. In contrast to the in vitro data, production of IFN-α in the sera of IFNR-deficient mice was still detectable and exhibited a partial impairment at 6 h posttreatment (Fig. 3C). These results suggest that production of type I IFN in vitro in response to AcNPV is regulated mainly by an IFNR-mediated signal pathway, whereas an IFNR-independent pathway is additionally involved in the production of type I IFN in response to AcNPV in vivo.

Envelope glycoprotein gp64 does not participate in the immune activation by AcNPV. A previous study demonstrated that the recombinant envelope glycoprotein of AcNPV lacking a transmembrane domain (gp64ΔTM) did not produce proinflammatory cytokines or type I IFN in a murine macrophage cell line, RAW264.7 (1). However, the ability of gp64ΔTM to induce an innate immune response in primary mouse immune cells and nonimmune cells has not yet been examined. To determine the involvement of the envelope glycoprotein of AcNPV in immune activation, we prepared a C-terminally six-His-tagged gp64 lacking the transmembrane region (His-gp64ΔTM), as described previously (1), and examined its ability to activate primary mouse cells, such as PECs, splenic $CD11c^+$ DCs, and MEFs. His-gp64ΔTM was purified as a homogeneous band and was clearly detected by anti-His and anti-gp64 antibodies (Fig. 4A). Although infection with

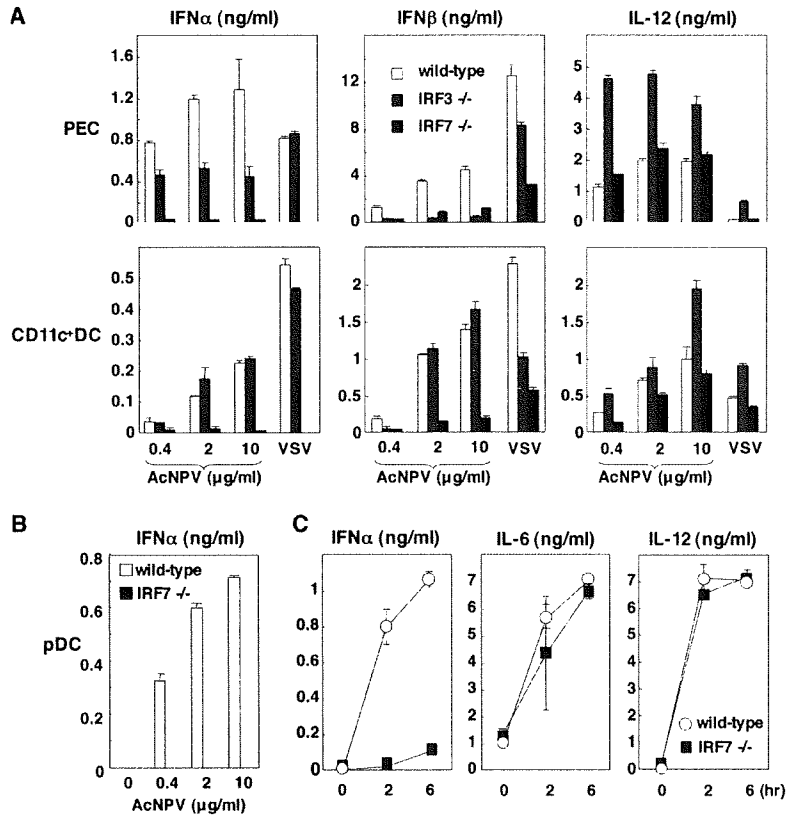

FIG. 2. IRF7 plays a crucial role in the production of type I IFN by AcNPV in immune cells and in mice. (A) PECs and splenic CD11c$^+$ DCs (2×10^5 cells/well) prepared from wild-type, IRF3-deficient, or IRF7-deficient mice were stimulated with the indicated amounts of AcNPV or VSV (NCP mutant, MOI of 0.1). After 24 h of incubation, the production of IFN-α, IFN-β, and IL-12 in culture supernatants was determined by ELISA. (B) Splenic pDCs (2×10^5 cells/well) prepared from wild-type or IRF7-deficient mice were stimulated with the indicated amounts of AcNPV. After 24 h of incubation, production of IFN-α in culture supernatants was determined by ELISA. (C) AcNPV (100 μg/mouse) was intraperitoneally inoculated into wild-type and IRF7-deficient mice, and levels of IL-12, IL-6, and IFN-α production in sera were determined by ELISA at the indicated times. Data are shown as the means ± standard deviations.

AcNPV produced large amounts of IL-12 and IFN-α in PECs and splenic CD11c$^+$ DCs, only a low level of IL-12 production was detected after infection with His-gp64ΔTM (Fig. 4B). Furthermore, infection with AcNPV resulted in rapid production of IFN-β, inflammatory cytokines, and chemokines, including IL-6, MCP-1, RANTES, and IP-10, in MEFs, in contrast to the low level of production of the cytokines by infection with His-gp64ΔTM (Fig. 4C). These results suggest that the envelope glycoprotein, gp64, does not play an important role in the immune activation by AcNPV.

AcNPV produces IFN-β and IFN-inducible chemokines through a TLR-independent and IRF3-dependent pathway in MEFs. We next examined the involvement of the TLR signaling pathway in immune activation by AcNPV in MEFs. MEFs were isolated from wild-type and MyD88/TRIF double knockout mice, and the production of cytokines after stimulation with AcNPV, VSV, LPS, or poly(I:C) was determined by ELISA and real-time PCR. In the MyD88/TRIF-deficient MEFs, the production of IL-6 was severely impaired in response to AcNPV and LPS, whereas no effect was observed after treatment with VSV or poly(I:C) (Fig. 5A, top). In contrast, the production of IFN-β in MEFs in response to AcNPV, VSV, or poly(I:C) was not affected by knockout of the MyD88/TRIF genes. LPS did not induce IFN-β production in either wild-type or MyD88/TRIF-deficient MEFs (Fig. 5A, bottom). Comparable levels of mRNA of IFN-β and IFN-inducible chemokines, including MCP-1, RANTES, and IP-10, were detected in wild-type and MyD88/TRIF knockout MEFs in response to AcNPV (Fig. 5B). These results suggest that a TLR-dependent pathway participates in the production of proinflammatory cytokines by AcNPV in MEFs, as seen with the immune cells, while AcNPV produces IFN-β and IFN-inducible chemokines in MEFs through a TLR-independent pathway.

Next, to determine the involvement of IRF3 and IRF7 in the immune activation in MEFs by AcNPV, wild-type and IRF3- or IRF7-deficient MEFs were treated with AcNPV, LPS, or VSV, and the production of cytokines was determined by ELISA and real-time PCR. Production of IL-6 in IRF3 or IRF7 knockout MEFs after treatment with AcNPV, VSV, or LPS was comparable to that in wild-type MEFs (Fig. 5C, top). In contrast, production of IFN-β was impaired in IRF3- and IRF7-deficient MEFs in response to AcNPV and VSV, respectively, while LPS induced no IFN production in either type of

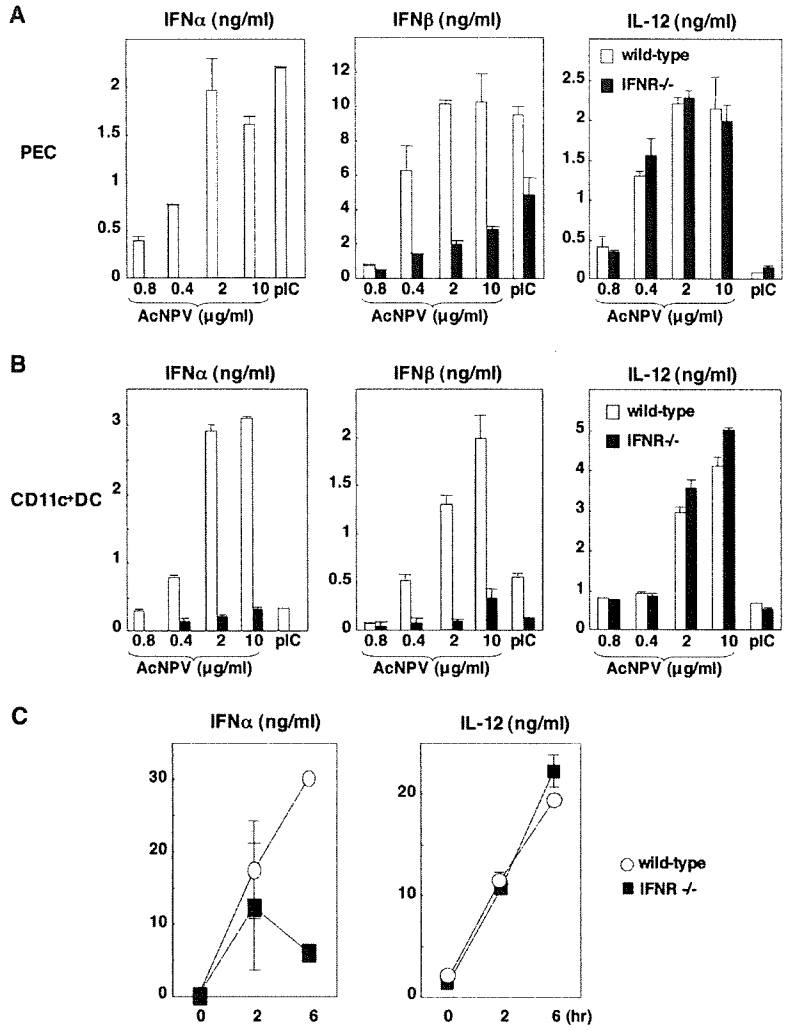

FIG. 3. Involvement of the IFNR signaling pathway in the production of type I IFN by AcNPV. (A and B) PECs (A) and splenic CD11c$^+$ DCs (B) (2×10^5 cells/well) prepared from wild-type and IFNR-deficient mice were stimulated with the indicated amounts of AcNPV or poly(I:C) (pIC) (50 μg/ml). After 24 h of incubation, the production of IFN-α, IFN-β, or IL-12 in culture supernatants was determined by ELISA. (C) AcNPV (100 μg/mouse) was intraperitoneally inoculated into wild-type and IFNR-deficient mice, and levels of IFN-α and IL-12 production in sera were determined by ELISA at the indicated time points. Data are shown as the means ± standard deviations.

MEF (Fig. 5C, bottom). Although robust transcription of IFN-β and IFN-inducible chemokines in response to AcNPV was detected in wild-type and IRF7-deficient MEFs, transcription of the genes in response to AcNPV was severely impaired in IRF3-deficient MEFs (Fig. 5D). These results indicate that AcNPV induces the production of IFN-β and IFN-inducible chemokines through a TLR-independent and IRF3-dependent pathway in MEFs, in contrast to the TLR-dependent and IRF3/IRF7-independent production of IL-6.

AcNPV induces antiviral status in MEFs through an IRF3-dependent pathway. To further examine the involvement of IRF3 in the induction of antiviral status in MEFs in response to AcNPV, wild-type and IRF3-deficient MEFs were transfected with the baculoviral DNA, and the mRNAs of the cytokines were measured. Transcription of IFN-β, IFN-α1, MCP-1, RANTES, and IP-10, but not that of IL-6, was impaired in IRF3-deficient MEFs upon transfection with baculoviral DNA (Fig. 6A).

To determine the involvement of endosomal maturation in the immune activation by AcNPV, the effect of chloroquine on the production of IFN-β and IL-6 in response to AcNPV or LPS was examined. Pretreatment with chloroquine reduced the secretion of IFN-β and IL-6 in MEFs in a dose-dependent manner in response to AcNPV infection but exhibited no effect on IL-6 production in MEFs by LPS treatment (Fig. 6B), suggesting that the impairment of IFN-β and IL-6 production was not due to the cytotoxicity of chloroquine. These results indicate that endosomal maturation is required for the induction of the innate immune response by AcNPV in MEFs.

Next, to determine the antiviral effects of the immune acti-

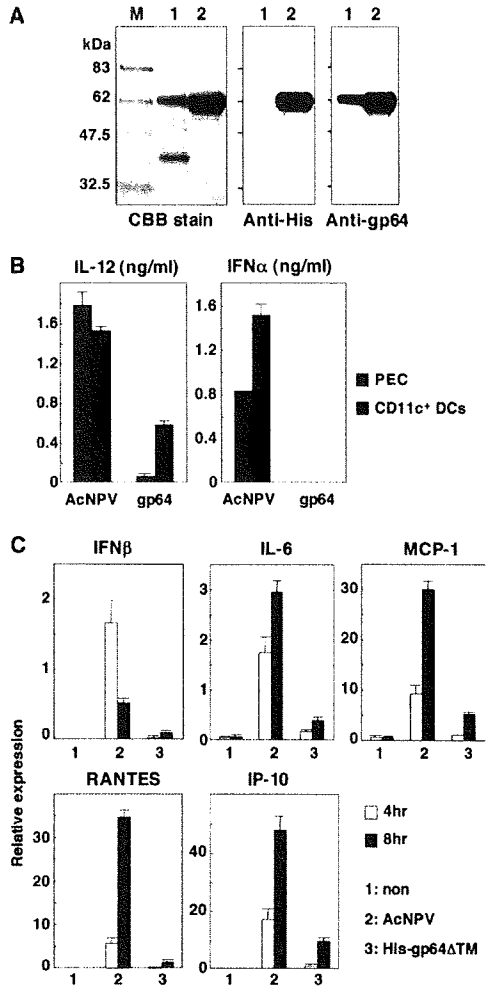

FIG. 4. Immune activation by AcNPV is not mediated by gp64. (A) His-gp64ΔTM expressed in Sf-9 cells was purified and subjected to sodium dodecyl sulfate-12.5% polyacrylamide gel electrophoresis under reducing conditions. Molecular size markers (lane M), purified AcNPV particles (lanes 1), and His-gp64ΔTM (lanes 2) were visualized by Coomassie blue (CBB) staining (left) and immunoblotting using antihexahistidine monoclonal antibody (middle) and anti-gp64 antibody (AcV5) (right). (B) PECs and splenic CD11c$^+$ DCs (2×10^5 cells/well) prepared from wild-type mice were stimulated with AcNPV (10 μg/ml) or His-gp64ΔTM (gp64) (20 μg/ml). After 24 h of incubation, production of IL-12 and IFN-α in culture supernatants was determined by ELISA. (C) MEFs (3×10^5 cells/well) prepared from wild-type mice were stimulated with AcNPV (10 μg/ml) or His-gp64ΔTM (20 μg/ml). At 4 h or 8 h poststimulation, total RNA was extracted and expression of mRNA of IFN-β, IL-6, MCP-1, RANTES, and IP-10 was determined by real-time PCR. Data are shown as the means ± standard deviations.

vation by AcNPV in MEFs, wild-type MEFs were pretreated with AcNPV or poly(I:C) and challenged with VSV (GLPLF mutant). Pretreatment with AcNPV (0.016 μg/ml to 2 μg/ml) or poly(I:C) (0.2 μg/ml to 25 μg/ml) conferred antiviral status against VSV infection in MEFs in a dose-dependent manner (Fig. 6C, left, and E). However, the induction of antiviral status by AcNPV or poly(I:C) treatment was completely abrogated in IRF3-deficient MEFs (Fig. 6C, right). On the other hand, pretreatment with IFN-α (10^1 to 10^4 U/ml) conferred antiviral status against VSV infection in both IRF knockout MEFs in a dose-dependent manner (Fig. 6D). These results clearly indicate that IRF3 plays a crucial role in the induction of antiviral status in MEFs by AcNPV.

Involvement of a TLR- and RIG-I/IPS-1-independent signaling pathway in immune activation by AcNPV. TLR3 has been shown to recognize viral dsRNA as well as a synthetic dsRNA analogue, poly(I:C), in the intracellular compartment. Recently, RIG-I and MDA5 have been identified as TLR-independent cytoplasmic RNA detectors and shown to induce type I IFN production through an adaptor molecule, IPS-1, that localizes in mitochondria (26, 36, 42, 47). To examine the involvement of TLR-independent cytoplasmic DNA-sensing machinery in the immune activation by AcNPV, as seen in the recognition of intracellular RNA, the production of type I IFN and IFN-inducible chemokines in PECs and splenic CD11c$^+$ DCs derived from RIG-I-, MDA5-, or IPS-1-deficient mice was examined. Type I IFN production in PECs and splenic CD11c$^+$ DCs in response to VSV and poly(I:C) was impaired by knockout of IPS-1, whereas AcNPV produced a significant amount of the IFNs in the IPS-1 knockout immune cells (Fig. 7A). Furthermore, IFN production in the immune cells in response to VSV was abrogated by knockout of the RIG-I gene but not by knockout of the MDA5 gene; however, AcNPV produced significant amounts of the IFNs in the RIG-I or MDA5 knockout immune cells (data not shown).

Next, to determine whether IPS-1 is involved in the production of type I IFN and IFN-inducible chemokines in MEFs in response to AcNPV, production of the cytokines in the IPS-1-deficient MEFs in response to VSV or AcNPV was examined (Fig. 7B). Production of IFN-β, IL-6, MCP-1, RANTES, and IP-10 was severely impaired in IPS-1-deficient MEFs upon VSV infection, whereas AcNPV produced substantial amounts of the cytokines in the IPS-1-deficient MEFs in spite of a slight reduction in IFN-β and IL-6 production (Fig. 7B). Similarly, production of the IFN-inducible chemokines in MEFs infected with VSV, but not with AcNPV, was also severely impaired by knockout of the RIG-I gene (data not shown). Collectively, these results suggest that a novel TLR- and RIG-I/IPS-1-independent signaling pathway(s) participated in the production of type I IFN and the IFN-inducible chemokines in both immunocompetent cells and MEFs in response to AcNPV infection.

DISCUSSION

Recent progress has been made in the identification of receptors, signal transduction molecules, and transcription factors that are required for the induction of type I IFN in cells upon infection with RNA and DNA viruses, as well as for the robust IFN production in pDCs, suggesting the presence of multiple signaling pathways for type I IFN induction (17, 23, 25). Production of type I IFN was shown to be induced through a number of different pathways in a cell-type-specific manner upon infection with HSV (40), although the precise mechanisms involved in sensing the foreign DNA of microorganisms remain largely unknown. In this study, we have examined the molecular mechanisms of type I IFN induction by AcNPV infection both in professional immune cells, including pDCs,

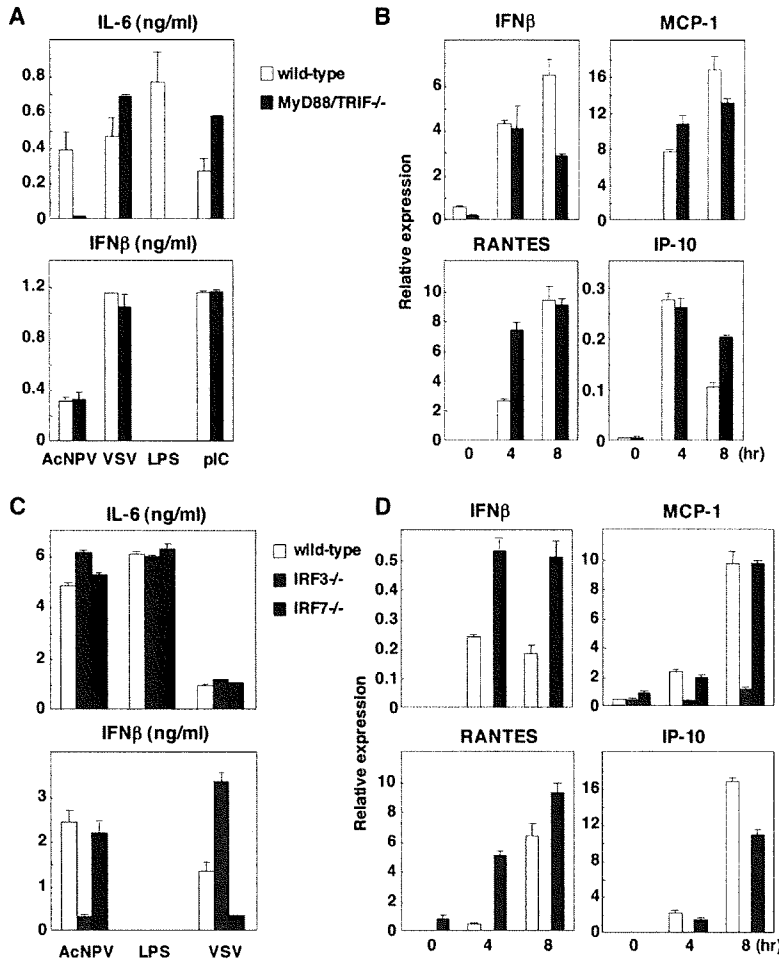

FIG. 5. AcNPV produces IFN-β and IFN-inducible chemokines through a TLR-independent and IRF3-dependent pathways in MEFs. (A) MEFs (2×10^4 cells/well) prepared from wild-type or MyD88/TRIF double knockout mice were stimulated with AcNPV (10 μg/ml), VSV (NCP mutant, MOI of 0.1), LPS (10 μg/ml), or poly(I:C) (pIC) (50 μg/ml). After 24 h of incubation, production of IL-6 and IFN-β in culture supernatants was determined by ELISA. (B) MEFs (3×10^5 cells/well) prepared from wild-type or MyD88/TRIF double knockout mice were stimulated with AcNPV (10 μg/ml). Total RNA was extracted at the indicated time points, and the expression of mRNA of IFN-β, MCP-1, RANTES, and IP-10 was determined by real-time PCR. (C) MEFs (2×10^4 cells/well) prepared from wild-type, IRF3-deficient, or IRF7-deficient mice were stimulated with AcNPV (10 μg/ml), LPS (10 μg/ml), or VSV (NCP mutant, MOI of 0.1). After 24 h of incubation, the production of IL-6 and IFN-β in culture supernatants was determined by ELISA. (D) MEFs (3×10^5 cells/well) prepared from wild-type, IRF3-deficient, or IRF7-deficient mice were stimulated with AcNPV (10 μg/ml). Total RNA was extracted at the indicated time points, and the expression of mRNA of IFN-β, MCP-1, RANTES, and IP-10 was determined by real-time PCR. Data are shown as the means ± standard deviations.

PECs, and splenic $CD11c^+$ DCs, and in nonimmune cells and raised the possibility of the involvement of a novel TLR- and IPS-1-independent pathway in the production of type I IFN in vitro as well as in vivo in response to AcNPV infection.

The frequency of bioactive CpG motifs capable of inducing immune activation through a TLR9-dependent pathway in the AcNPV genome was similar to that in *E. coli* and HSV and was significantly higher than that in entomopoxvirus (1, 51). Furthermore, it was shown that HSV and murine cytomegalovirus produce inflammatory cytokines and type I IFN through both TLR9-dependent and -independent pathways (7, 15, 29, 32, 44). Recently, it was also reported that adenovirus DNA produced IL-6 and IFN-α through an entirely TLR/MyD88-independent pathway in non-pDCs (53), although the presence of the CpG motifs in the adenoviral genome has not yet been determined. The current model of TLR9 activation by viral DNA is as follows. The virus particles are internalized into cells and degraded within the endocytic vesicles, and the digested viral genome subsequently actives TLR9 localized in the endosomal compartments. Treatment with inhibitors for endosomal maturation or acidification efficiently inhibits TLR7 and TLR9 activation by viral RNA and DNA, respectively (8, 32, 33). Interestingly, the production of type I IFN in PECs upon infection with AcNPV was resistant to pretreatment with endocytosis inhibitors, suggesting that the cytoplasmic recognition of AcNPV by TLR-independent immune sensors may be required for type I IFN production in PECs. The purified AcNPV DNA encapsulated in liposomes induced the produc-

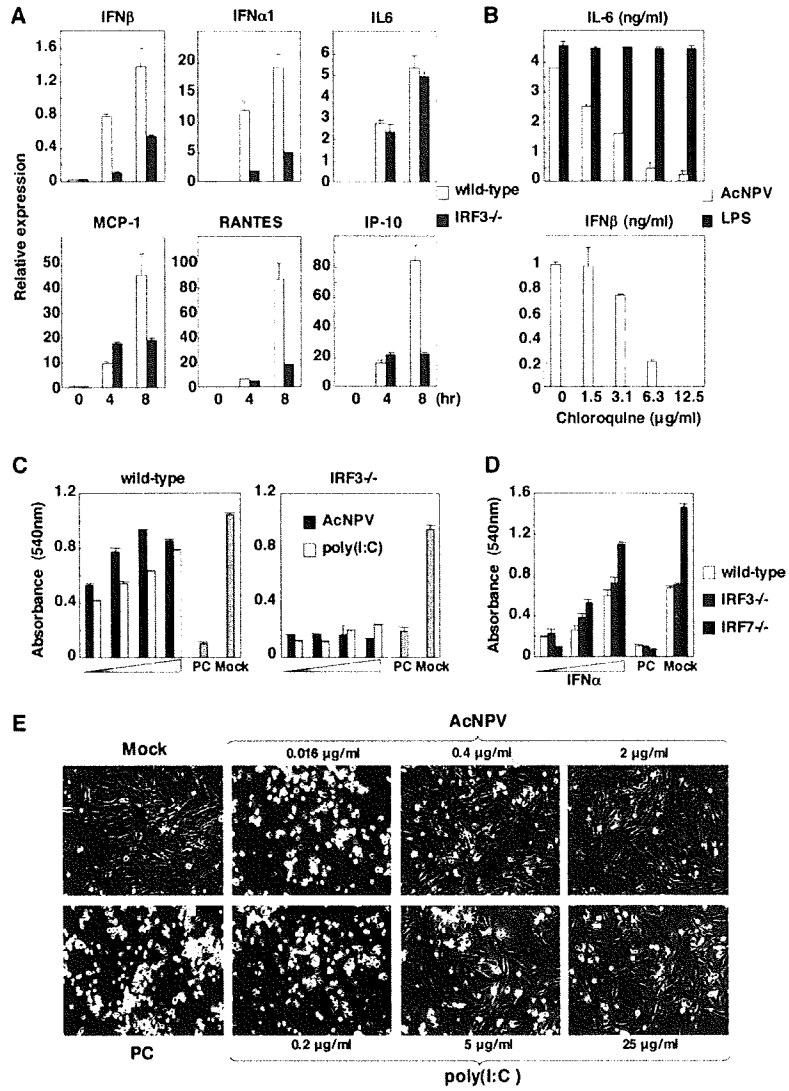

FIG. 6. AcNPV induces antiviral status in MEFs through an IRF3-dependent pathway. (A) MEFs (3×10^5 cells/well) prepared from wild-type and IRF3-deficient mice were transfected with AcNPV DNA (25 μg/ml). Total RNA was extracted at the indicated time points, and the expression of mRNA of IFN-β, IFN-α1, MCP-1, RANTES, IL-6, and IP-10 was determined by real-time PCR. (B) MEFs (2×10^4 cells/well) prepared from wild-type mice were stimulated with AcNPV (10 μg/ml) or LPS (10 μg/ml) in the presence of the indicated concentrations of chloroquine. After 24 h of incubation, production of IL-6 and IFN-β in culture supernatants was determined by ELISA. (C) MEFs (2×10^4 cells/well) prepared from wild-type and IRF3-deficient mice were incubated with AcNPV (0.016 μg/ml to 2 μg/ml) or poly(I:C) (0.2 μg/ml to 25 μg/ml). After 24 h of incubation, cells were washed extensively with warm medium and infected with VSV (GLPLF mutant, MOI of 0.1). Cell viability was determined at 24 h postinfection by crystal violet staining and quantitated by spectroscopy. (D) MEFs (2×10^4 cells/well) prepared from wild-type, IRF3-deficient, or IRF7-deficient mice were incubated with serial dilutions of murine IFN-α (10^1 to 10^4 U/ml). After 24 h of incubation, cells were washed extensively with warm medium and infected with VSV (GLPLF strain, MOI of 0.1). Cell viability was determined at 24 h postinfection by crystal violet staining and quantitated by spectroscopy. Values are plotted as means from the triplicate wells. Data are shown as means ± standard deviations. (E) Microscopic observation of MEFs from wild-type mice, showing the antiviral status against VSV infection by the treatment with AcNPV or poly(I:C) in a dose-dependent manner. PC, infected cells; Mock, mock-infected cells. Samples are shown at a magnification of ×40.

tion of type I IFN through both TLR9/MyD88-dependent and -independent pathways in PECs. These results indicate that the genomic DNA of AcNPV is recognized by at least two different pathways, TLR9-dependent endosomal recognition and TLR9-independent cytoplasmic recognition, and that type I IFN production by AcNPV is totally dependent on the latter process. However, the precise mechanisms of the immune activation of immunocompetent cells by AcNPV DNA through a TLR-independent pathway remain unknown. Therefore, further studies are needed to determine the molecular mechanisms underlying the type I IFN production through a TLR-independent cytoplasmic sensor for baculovirus DNA.

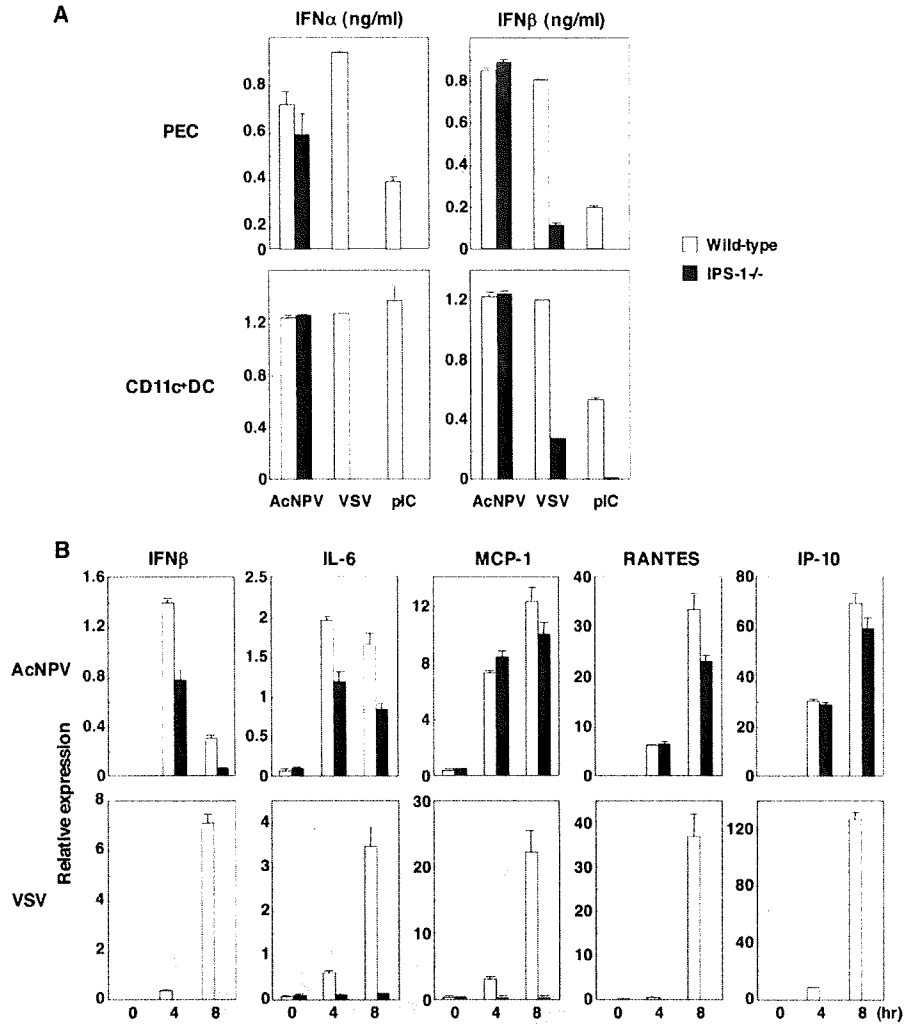

FIG. 7. Role of IPS-1 in immune activation by AcNPV. (A) PECs and splenic CD11c$^+$ DCs (2×10^5 cells/well) prepared from wild-type and IPS-1-deficient mice were stimulated with AcNPV (10 μg/ml), VSV (NCP mutant, MOI of 0.1), or poly(I:C) (pIC) (50 μg/ml). After 24 h of incubation, production of IFN-α and IFN-β in culture supernatants was determined by ELISA. (B) MEFs (3×10^5 cells/well) prepared from wild-type and IPS-1-deficient mice were stimulated with AcNPV (10 μg/ml) or VSV (NCP mutant, MOI of 0.1). Total RNA was extracted at the indicated time points, and the expression of mRNA of IFN-β, MCP-1, RANTES, IL-6, and IP-10 was determined by real-time PCR. Data are shown as the means ± standard deviations.

A novel TLR-independent cytosolic surveillance system for transfected dsDNA that elicits type I IFN induction through a TANK binding kinase 1 (TBK1)/IκB kinase-related kinase (IKKi)/IRF3 pathway has been shown to exist (19, 43). Our preliminary data also indicate that type I IFN production was severely reduced in TBK1-deficient MEFs in response to AcNPV and insufficient to protect cells from VSV infection (data not shown), suggesting the involvement of TBK1 in AcNPV-induced immune activation. Recently, a cytoplasmic recognition receptor, DAI (DNA-dependent activator of IRFs), was shown to be activated by dsDNA from a variety of sources and to produce type I IFN through an IRF3 and probably IRF7 pathway (45). However, there are conflicting reports suggesting a lack of impairment of type I IFN production in DAI knockout mice and DAI knockdown murine macrophages or MEFs in response to dsDNA of synthetic B-form DNA and from bacteria (4, 20). In this study, we have shown that splenic CD11c$^+$ DCs derived from IRF3-deficient mice produced a level of type I IFN compatible with that in wild-type mice in response to AcNPV, in contrast to the lack of IFN-β production in the PECs derived from the IRF3-deficient mice. More recently, two groups reported the identification of a membrane protein, termed mitochondrial mediator of IRF3 activation (MITA) or stimulator of IFN genes (STING), that activates IRF3 to induce a type I IFN response to viral infection (21, 52). Although both groups described slightly different characterizations of MITA, or STING, in terms of localization and signal transduction, both groups exhibited the opinion that MITA or STING plays a critical role in type I IFN production by B-form DNA. Although DAI-mediated type I IFN production was more

dependent on IRF3 than on IRF7, the cytoplasmic DNA sensors, including DAI and MITA or STING, may participate in the induction of type I IFN upon infection with AcNPV.

In the cytoplasm, RIG-I and MDA5 are critically involved in the recognition of dsRNA, and the adaptor molecule IPS-1 interacts with RIG-I and MDA5 to facilitate TBK1- and IKKi-mediated IRF3 and IRF7 activation, which leads to termination of the replication of RNA viruses through the helicase function. In addition, RIG-I has been shown to discriminate viral RNAs from the vast number and variety of cellular RNAs by recognizing a terminal 5′ triphosphate, but not 5′ OH or a 5′ methylguanosine cap (37, 39). In this study, both RIG-I- and IPS-1-deficient MEFs but not immunocompetent cells partially impaired the production of IFN-β and IL-6, but not that of MCP-1, RANTES, and IP-10, in response to AcNPV, suggesting the possible generation of dsRNA in MEFs upon infection with AcNPV in spite of the lack of replication. Although there is no evidence for the functional expression of the viral proteins, transcription of immediate-early genes of baculovirus was detected in HeLa and BHK cells upon infection with AcNPV by DNA microarray analysis (10) and in HEK293 cells and rat primary Schwann cells upon infection with *Bombyx mori* NPV by reverse transcription-PCR (27). These reports are consistent with our observations that the RIG-I/IPS-1 pathway partially participates in type I IFN induction by AcNPV infection in MEFs.

We have shown previously that an intranasal inoculation of AcNPV induces protective immunity from a lethal challenge of influenza A virus in mice (2) and that AcNPV produces type I IFN in immune cells of mice via a TLR9/MyD88-independent pathway (1). Our present studies further confirmed that AcNPV induces a strong antiviral immunity through a TLR-independent pathway. Although further studies are needed to clarify the precise mechanisms underlying the antiviral responses, a TLR-independent and probably TBK1-IRF3/IRF7-dependent signaling pathway may contribute to the induction of protective immunity against viral challenge induced by AcNPV infection in vivo.

ACKNOWLEDGMENTS

We thank H. Murase for her secretarial work.

This work was supported in part by grants-in-aid from the Research and Development Program for New Bio-industry Initiatives of Bio-oriented Technology Research Advancement Institution (BRAIN) and the Ministry of Education, Culture, Sports, Science, and Technology, Japan.

We have no conflicting financial interests.

REFERENCES

1. **Abe, T., H. Hemmi, H. Miyamoto, K. Moriishi, S. Tamura, H. Takaku, S. Akira, and Y. Matsuura.** 2005. Involvement of the Toll-like receptor 9 signaling pathway in the induction of innate immunity by baculovirus. J. Virol. **79**:2847–2858.
2. **Abe, T., H. Takahashi, H. Hamazaki, N. Miyano-Kurosaki, Y. Matsuura, and H. Takaku.** 2003. Baculovirus induces an innate immune response and confers protection from lethal influenza virus infection in mice. J. Immunol. **171**:1133–1139.
3. **Bjorck, P.** 2001. Isolation and characterization of plasmacytoid dendritic cells from Flt3 ligand and granulocyte-macrophage colony-stimulating factor-treated mice. Blood **98**:3520–3526.
4. **Charrel-Dennis, M., E. Latz, K. A. Halmen, P. Trieu-Cuot, K. A. Fitzgerald, D. L. Kasper, and D. T. Golenbock.** 2008. TLR-independent type I interferon induction in response to an extracellular bacterial pathogen via intracellular recognition of its DNA. Cell Host Microbe **4**:543–554.
5. **Chessler, A. D., L. R. Ferreira, T. H. Chang, K. A. Fitzgerald, and B. A. Burleigh.** 2008. A novel IFN regulatory factor 3-dependent pathway activated by trypanosomes triggers IFN-beta in macrophages and fibroblasts. J. Immunol. **181**:7917–7924.
6. **Coccia, E. M., M. Severa, E. Giacomini, D. Monneron, M. E. Remoli, I. Julkunen, M. Cella, R. Lande, and G. Uze.** 2004. Viral infection and Toll-like receptor agonists induce a differential expression of type I and lambda interferons in human plasmacytoid and monocyte-derived dendritic cells. Eur. J. Immunol. **34**:796–805.
7. **Delale, T., A. Paquin, C. Asselin-Paturel, M. Dalod, G. Brizard, E. E. Bates, P. Kastner, S. Chan, S. Akira, A. Vicari, C. A. Biron, G. Trinchieri, and F. Briere.** 2005. MyD88-dependent and -independent murine cytomegalovirus sensing for IFN-alpha release and initiation of immune responses in vivo. J. Immunol. **175**:6723–6732.
8. **Diebold, S. S., T. Kaisho, H. Hemmi, S. Akira, and C. Reis e Sousa.** 2004. Innate antiviral responses by means of TLR7-mediated recognition of single-stranded RNA. Science **303**:1529–1531.
9. **Diebold, S. S., M. Montoya, H. Unger, L. Alexopoulou, P. Roy, L. E. Haswell, A. Al-Shamkhani, R. Flavell, P. Borrow, and C. Reis e Sousa.** 2003. Viral infection switches non-plasmacytoid dendritic cells into high interferon producers. Nature **424**:324–328.
10. **Fujita, R., T. Matsuyama, J. Yamagishi, K. Sahara, S. Asano, and H. Bando.** 2006. Expression of *Autographa californica* multiple nucleopolyhedrovirus genes in mammalian cells and upregulation of the host beta-actin gene. J. Virol. **80**:2390–2395.
11. **Gilliet, M., W. Cao, and Y. J. Liu.** 2008. Plasmacytoid dendritic cells: sensing nucleic acids in viral infection and autoimmune diseases. Nat. Rev. Immunol. **8**:594–606.
12. **Gronowski, A. M., D. M. Hilbert, K. C. Sheehan, G. Garotta, and R. D. Schreiber.** 1999. Baculovirus stimulates antiviral effects in mammalian cells. J. Virol. **73**:9944–9951.
13. **Hemmi, H., O. Takeuchi, T. Kawai, T. Kaisho, S. Sato, H. Sanjo, M. Matsumoto, K. Hoshino, H. Wagner, K. Takeda, and S. Akira.** 2000. A Toll-like receptor recognizes bacterial DNA. Nature **408**:740–745.
14. **Hervas-Stubbs, S., P. Rueda, L. Lopez, and C. Leclerc.** 2007. Insect baculoviruses strongly potentiate adaptive immune responses by inducing type I IFN. J. Immunol. **178**:2361–2369.
15. **Hochrein, H., B. Schlatter, M. O'Keeffe, C. Wagner, F. Schmitz, M. Schiemann, S. Bauer, M. Suter, and H. Wagner.** 2004. Herpes simplex virus type-1 induces IFN-alpha production via Toll-like receptor 9-dependent and -independent pathways. Proc. Natl. Acad. Sci. USA **101**:11416–11421.
16. **Honda, K., and T. Taniguchi.** 2006. IRFs: master regulators of signalling by Toll-like receptors and cytosolic pattern-recognition receptors. Nat. Rev. Immunol. **6**:644–658.
17. **Honda, K., H. Yanai, T. Mizutani, H. Negishi, N. Shimada, N. Suzuki, Y. Ohba, A. Takaoka, W. C. Yeh, and T. Taniguchi.** 2004. Role of a transductional-transcriptional processor complex involving MyD88 and IRF-7 in Toll-like receptor signaling. Proc. Natl. Acad. Sci. USA **101**:15416–15421.
18. **Honda, K., H. Yanai, H. Negishi, M. Asagiri, M. Sato, T. Mizutani, N. Shimada, Y. Ohba, A. Takaoka, N. Yoshida, and T. Taniguchi.** 2005. IRF-7 is the master regulator of type-I interferon-dependent immune responses. Nature **434**:772–777.
19. **Ishii, K. J., C. Coban, H. Kato, K. Takahashi, Y. Torii, F. Takeshita, H. Ludwig, G. Sutter, K. Suzuki, H. Hemmi, S. Sato, M. Yamamoto, S. Uematsu, T. Kawai, O. Takeuchi, and S. Akira.** 2006. A Toll-like receptor-independent antiviral response induced by double-stranded B-form DNA. Nat. Immunol. **7**:40–48.
20. **Ishii, K. J., T. Kawagoe, S. Koyama, K. Matsui, H. Kumar, T. Kawai, S. Uematsu, O. Takeuchi, F. Takeshita, C. Coban, and S. Akira.** 2008. TANK-binding kinase-1 delineates innate and adaptive immune responses to DNA vaccines. Nature **451**:725–729.
21. **Ishikawa, H., and G. N. Barber.** 2008. STING is an endoplasmic reticulum adaptor that facilitates innate immune signalling. Nature **455**:674–678.
22. **Jayakar, H. R., and M. A. Whitt.** 2002. Identification of two additional translation products from the matrix (M) gene that contribute to vesicular stomatitis virus cytopathology. J. Virol. **76**:8011–8018.
23. **Kato, H., S. Sato, M. Yoneyama, M. Yamamoto, S. Uematsu, K. Matsui, T. Tsujimura, K. Takeda, T. Fujita, O. Takeuchi, and S. Akira.** 2005. Cell type-specific involvement of RIG-I in antiviral response. Immunity **23**:19–28.
24. **Kawai, T., and S. Akira.** 2006. Innate immune recognition of viral infection. Nat. Immunol. **7**:131–137.
25. **Kawai, T., S. Sato, K. J. Ishii, C. Coban, H. Hemmi, M. Yamamoto, K. Terai, M. Matsuda, J. Inoue, S. Uematsu, O. Takeuchi, and S. Akira.** 2004. Interferon-alpha induction through Toll-like receptors involves a direct interaction of IRF7 with MyD88 and TRAF6. Nat. Immunol. **5**:1061–1068.
26. **Kawai, T., K. Takahashi, S. Sato, C. Coban, H. Kumar, H. Kato, K. J. Ishii, O. Takeuchi, and S. Akira.** 2005. IPS-1, an adaptor triggering RIG-I- and Mda5-mediated type I interferon induction. Nat. Immunol. **6**:981–988.
27. **Kenoutis, C., R. C. Efrose, L. Swevers, A. A. Lavdas, M. Gaitanou, R. Matsas, and K. Iatrou.** 2006. Baculovirus-mediated gene delivery into mammalian cells does not alter their transcriptional and differentiating potential but is accompanied by early viral gene expression. J. Virol. **80**:4135–4146.
28. **Kost, T. A., J. P. Condreay, and D. L. Jarvis.** 2005. Baculovirus as versatile

vectors for protein expression in insect and mammalian cells. Nat. Biotechnol. **23**:567–575.
29. **Krug, A., G. D. Luker, W. Barchet, D. A. Leib, S. Akira, and M. Colonna.** 2004. Herpes simplex virus type 1 activates murine natural interferon-producing cells through toll-like receptor 9. Blood **103**:1433–1437.
30. **Kumar, H., T. Kawai, H. Kato, S. Sato, K. Takahashi, C. Coban, M. Yamamoto, S. Uematsu, K. J. Ishii, O. Takeuchi, and S. Akira.** 2006. Essential role of IPS-1 in innate immune responses against RNA viruses. J. Exp. Med. **203**:1795–1803.
31. **Luckow, V. A., and M. D. Summers.** 1988. Signals important for high-level expression of foreign genes in Autographa californica nuclear polyhedrosis virus expression vectors. Virology **167**:56–71.
32. **Lund, J., A. Sato, S. Akira, R. Medzhitov, and A. Iwasaki.** 2003. Toll-like receptor 9-mediated recognition of herpes simplex virus-2 by plasmacytoid dendritic cells. J. Exp. Med. **198**:513–520.
33. **Lund, J. M., L. Alexopoulou, A. Sato, M. Karow, N. C. Adams, N. W. Gale, A. Iwasaki, and R. A. Flavell.** 2004. Recognition of single-stranded RNA viruses by Toll-like receptor 7. Proc. Natl. Acad. Sci. USA **101**:5598–5603.
34. **Malmgaard, L., J. Melchjorsen, A. G. Bowie, S. C. Mogensen, and S. R. Paludan.** 2004. Viral activation of macrophages through TLR-dependent and -independent pathways. J. Immunol. **173**:6890–6898.
35. **Matsuura, Y., R. D. Possee, H. A. Overton, and D. H. Bishop.** 1987. Baculovirus expression vectors: the requirements for high level expression of proteins, including glycoproteins. J. Gen. Virol. **68**:1233–1250.
36. **Meylan, E., J. Curran, K. Hofmann, D. Moradpour, M. Binder, R. Bartenschlager, and J. Tschopp.** 2005. Cardif is an adaptor protein in the RIG-I antiviral pathway and is targeted by hepatitis C virus. Nature **437**:1167–1172.
37. **Nallagatla, S. R., J. Hwang, R. Toroney, X. Zheng, C. E. Cameron, and P. C. Bevilacqua.** 2007. 5′-triphosphate-dependent activation of PKR by RNAs with short stem-loops. Science **318**:1455–1458.
38. **Nociari, M., O. Ocheretina, J. W. Schoggins, and E. Falck-Pedersen.** 2007. Sensing infection by adenovirus: Toll-like receptor-independent viral DNA recognition signals activation of the interferon regulatory factor 3 master regulator. J. Virol. **81**:4145–4157.
39. **Pichlmair, A., O. Schulz, C. P. Tan, T. I. Naslund, P. Liljestrom, F. Weber, and C. Reis e Sousa.** 2006. RIG-I-mediated antiviral responses to single-stranded RNA bearing 5′-phosphates. Science **314**:997–1001.
40. **Rasmussen, S. B., L. N. Sorensen, L. Malmgaard, N. Ank, J. D. Baines, Z. J. Chen, and S. R. Paludan.** 2007. Type I interferon production during herpes simplex virus infection is controlled by cell-type-specific viral recognition through Toll-like receptor 9, the mitochondrial antiviral signaling protein pathway, and novel recognition systems. J. Virol. **81**:13315–13324.
41. **Sato, M., H. Suemori, N. Hata, M. Asagiri, K. Ogasawara, K. Nakao, T. Nakaya, M. Katsuki, S. Noguchi, N. Tanaka, and T. Taniguchi.** 2000. Distinct and essential roles of transcription factors IRF-3 and IRF-7 in response to viruses for IFN-alpha/beta gene induction. Immunity **13**:539–548.
42. **Seth, R. B., L. Sun, C. K. Ea, and Z. J. Chen.** 2005. Identification and characterization of MAVS, a mitochondrial antiviral signaling protein that activates NF-kappaB and IRF 3. Cell **122**:669–682.
43. **Stetson, D. B., and R. Medzhitov.** 2006. Recognition of cytosolic DNA activates an IRF3-dependent innate immune response. Immunity **24**:93–103.
44. **Tabeta, K., P. Georgel, E. Janssen, X. Du, K. Hoebe, K. Crozat, S. Mudd, L. Shamel, S. Sovath, J. Goode, L. Alexopoulou, R. A. Flavell, and B. Beutler.** 2004. Toll-like receptors 9 and 3 as essential components of innate immune defense against mouse cytomegalovirus infection. Proc. Natl. Acad. Sci. USA **101**:3516–3521.
45. **Takaoka, A., Z. Wang, M. K. Choi, H. Yanai, H. Negishi, T. Ban, Y. Lu, M. Miyagishi, T. Kodama, K. Honda, Y. Ohba, and T. Taniguchi.** 2007. DAI (DLM-1/ZBP1) is a cytosolic DNA sensor and an activator of innate immune response. Nature **448**:501–505.
46. **Waibler, Z., M. Anzaghe, H. Ludwig, S. Akira, S. Weiss, G. Sutter, and U. Kalinke.** 2007. Modified vaccinia virus Ankara induces Toll-like receptor-independent type I interferon responses. J. Virol. **81**:12102–12110.
47. **Xu, L. G., Y. Y. Wang, K. J. Han, L. Y. Li, Z. Zhai, and H. B. Shu.** 2005. VISA is an adapter protein required for virus-triggered IFN-beta signaling. Mol. Cell **19**:727–740.
48. **Yamamoto, M., S. Sato, H. Hemmi, K. Hoshino, T. Kaisho, H. Sanjo, O. Takeuchi, M. Sugiyama, M. Okabe, K. Takeda, and S. Akira.** 2003. Role of adaptor TRIF in the MyD88-independent toll-like receptor signaling pathway. Science **301**:640–643.
49. **Yoneyama, M., M. Kikuchi, K. Matsumoto, T. Imaizumi, M. Miyagishi, K. Taira, E. Foy, Y. M. Loo, M. Gale, Jr., S. Akira, S. Yonehara, A. Kato, and T. Fujita.** 2005. Shared and unique functions of the DExD/H-box helicases RIG-I, MDA5, and LGP2 in antiviral innate immunity. J. Immunol. **175**:2851–2858.
50. **Yoneyama, M., M. Kikuchi, T. Natsukawa, N. Shinobu, T. Imaizumi, M. Miyagishi, K. Taira, S. Akira, and T. Fujita.** 2004. The RNA helicase RIG-I has an essential function in double-stranded RNA-induced innate antiviral responses. Nat. Immunol. **5**:730–737.
51. **Zheng, M., D. M. Klinman, M. Gierynska, and B. T. Rouse.** 2002. DNA containing CpG motifs induces angiogenesis. Proc. Natl. Acad. Sci. USA **99**:8944–8949.
52. **Zhong, B., Y. Yang, S. Li, Y. Y. Wang, Y. Li, F. Diao, C. Lei, X. He, L. Zhang, P. Tien, and H. B. Shu.** 2008. The adaptor protein MITA links virus-sensing receptors to IRF3 transcription factor activation. Immunity **29**:538–550.
53. **Zhu, J., X. Huang, and Y. Yang.** 2007. Innate immune response to adenoviral vectors is mediated by both Toll-like receptor-dependent and -independent pathways. J. Virol. **81**:3170–3180.

JOURNAL OF VIROLOGY, Mar. 2009, p. 2389–2392 Vol. 83, No. 5
0022-538X/09/$08.00+0 doi:10.1128/JVI.01690-08

Proteasomal Turnover of Hepatitis C Virus Core Protein Is Regulated by Two Distinct Mechanisms: a Ubiquitin-Dependent Mechanism and a Ubiquitin-Independent but PA28γ-Dependent Mechanism▽

Ryosuke Suzuki,[1] Kohji Moriishi,[2] Kouichirou Fukuda,[1] Masayuki Shirakura,[1] Koji Ishii,[1] Ikuo Shoji,[3] Takaji Wakita,[1] Tatsuo Miyamura,[1] Yoshiharu Matsuura,[2] and Tetsuro Suzuki[1]*

Department of Virology II, National Institute of Infectious Diseases, Tokyo 162-8640,[1] Department of Molecular Virology, Research Institute for Microbial Diseases, Osaka University, Osaka 565-0871,[2] and Division of Microbiology, Kobe University Graduate School of Medicine, Hyogo 650-0017,[3] Japan

Received 8 August 2008/Accepted 5 December 2008

We have previously reported on the ubiquitylation and degradation of hepatitis C virus core protein. Here we demonstrate that proteasomal degradation of the core protein is mediated by two distinct mechanisms. One leads to polyubiquitylation, in which lysine residues in the N-terminal region are preferential ubiquitylation sites. The other is independent of the presence of ubiquitin. Gain- and loss-of-function analyses using lysineless mutants substantiate the hypothesis that the proteasome activator PA28γ, a binding partner of the core, is involved in the ubiquitin-independent degradation of the core protein. Our results suggest that turnover of this multifunctional viral protein can be tightly controlled via dual ubiquitin-dependent and -independent proteasomal pathways.

Hepatitis C virus (HCV) core protein, whose amino acid sequence is highly conserved among different HCV strains, not only is involved in the formation of the HCV virion but also has a number of regulatory functions, including modulation of signaling pathways, cellular and viral gene expression, cell transformation, apoptosis, and lipid metabolism (reviewed in references 9 and 15). We have previously reported that the E6AP E3 ubiquitin (Ub) ligase binds to the core protein and plays an important role in polyubiquitylation and proteasomal degradation of the core protein (22). Another study from our group identified the proteasome activator PA28γ/REG-γ as an HCV core-binding partner, demonstrating degradation of the core protein via a PA28γ-dependent pathway (16, 17). In this work, we further investigated the molecular mechanisms underlying proteasomal degradation of the core protein and found that in addition to regulation by the Ub-mediated pathway, the turnover of the core protein is also regulated by PA28γ in a Ub-independent manner.

Although ubiquitylation of substrates generally requires at least one Lys residue to serve as a Ub acceptor site (5), there is no consensus as to the specificity of the Lys targeted by Ub (4, 8). To determine the sites of Ub conjugation in the core protein, we used site-directed mutagenesis to replace individual Lys residues or clusters of Lys residues with Arg residues in the N-terminal 152 amino acids (aa) of the core (C152), within which is contained all seven Lys residues (Fig. 1A). Plasmids expressing a variety of mutated core proteins were generated by PCR and inserted into the pCAGGS (18). Each core-expressing construct was transfected into human embryonic kidney 293T cells along with the pMT107 (25) encoding a Ub moiety tagged with six His residues (His_6). Transfected cells were treated with the proteasome inhibitor MG132 for 14 h to maximize the level of Ub-conjugated core intermediates by blocking the proteasome pathway and were harvested 48 h posttransfection. His_6-tagged proteins were purified from the extracts by Ni^{2+}-chelation chromatography. Eluted protein and whole lysates of transfected cells before purification were analyzed by Western blotting using anticore antibodies (Fig. 1B). Mutations replacing one or two Lys residues with Arg in the core protein did not affect the efficiency of ubiquitylation: detection of multiple Ub-conjugated core intermediates was observed in the mutant core proteins comparable to the results seen with the wild-type core protein as previously reported (23). In contrast, a substitution of four N-terminal Lys residues (C152K6-23R) caused a significant reduction in ubiquitylation (Fig. 1B, lane 9). Multiple Ub-conjugated core intermediates were not detected in the Lys-less mutant (C152KR), in which all seven Lys residues were replaced with Arg (Fig. 1B, lane 11). These results suggest that there is not a particular Lys residue in the core protein to act as the Ub acceptor but that more than one Lys located in its N-terminal region can serve as the preferential ubiquitylation site. In rare cases, Ub is known to be conjugated to the N terminus of proteins; however, these results indicate that this does not occur within the core protein.

To investigate how polyubiquitylation correlates with proteasome degradation of the core protein, we performed kinetic analysis of the wild-type and mutated core proteins by use of the Ub protein reference (UPR) technique, which can compensate for data scatter of sample-to-sample variations such as levels of expression (10, 24). Fusion proteins expressed from UPR-based constructs (Fig. 2A) were cotranslationally cleaved by deubiquitylating enzymes, thereby generating equimolar quantities of the core proteins and the reference protein, dihydrofolate reductase-hemagglutinin (DHFR-HA) tag-modified Ub, in which the Lys at aa 48 was replaced by Arg to prevent its polyubiquitylation (Ub^{R48}). After 24 h of transfec-

* Corresponding author. Mailing address: Department of Virology II, National Institute of Infectious Diseases, 1-23-1 Toyama, Shinjuku-ku, Tokyo 162-8640, Japan. Phone: 81-3-5285-1111. Fax: 81-3-5285-1161. E-mail: tesuzuki@nih.go.jp.

▽ Published ahead of print on 17 December 2008.

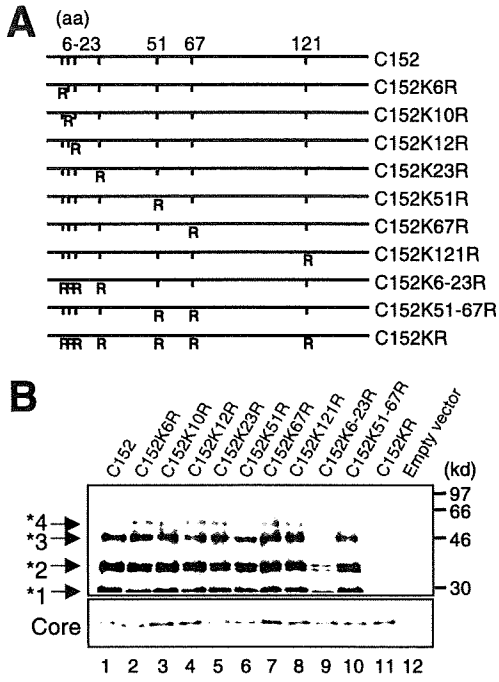

FIG. 1. In vivo ubiquitylation of HCV core protein. (A) The HCV core protein (N-terminal 152 aa) is represented on the top. The positions of the amino acid residues of the core protein are indicated above the bold lines. The positions of the seven Lys residues in the core are marked by vertical ticks. Substitution of Lys with Arg (R) is schematically depicted. (B) Detection of ubiquitylated forms of the core proteins. The transfected cells with core expression plasmids and pMT107 were treated with the proteasome inhibitor MG132 and harvested 48 h after transfection. His_6-tagged proteins were purified and subsequently analyzed by Western blot analysis using anticore antibody (upper panel). Core proteins conjugated to a number of His_6-Ub are denoted with asterisks. Whole lysates of transfected cells before purification were also analyzed (lower panel). Lanes 1 to 11, C152 to C152KR, as indicated for panel A. Lane 12; empty vector.

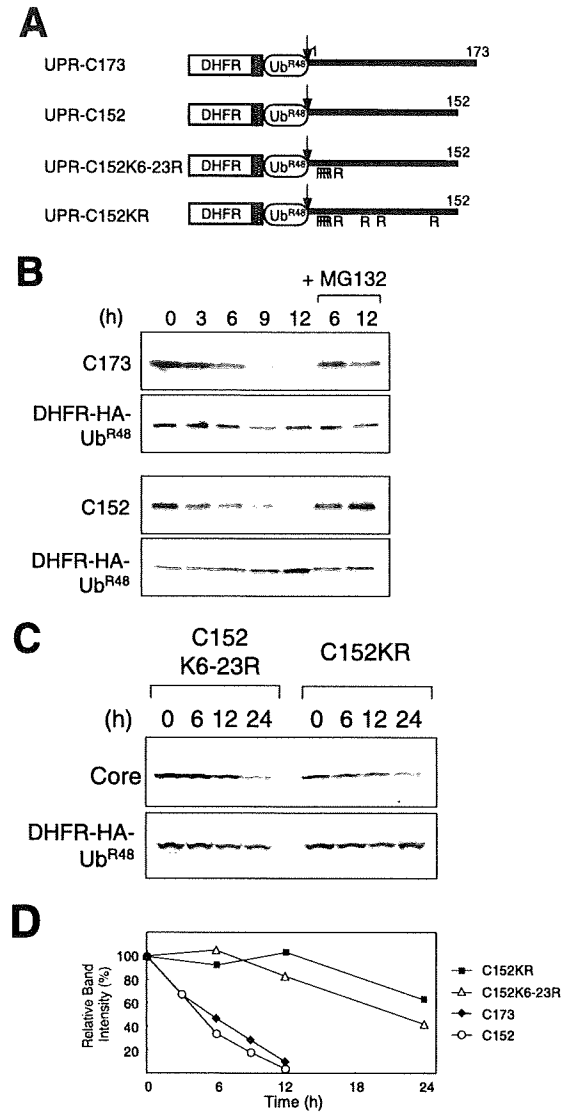

FIG. 2. Kinetic analysis of degradation of HCV core proteins. (A) The fusion constructs used in the UPR technique. Open boxes indicate the DHFR sequence, which is extended at the C terminus by a sequence containing the HA epitope (hatched boxes). Ub^{R48} moieties bearing the Lys-Arg substitution at aa 48 are represented by open ellipses. Bold lines indicate the regions of the core protein. The amino acid positions of the core protein are indicated above the bold lines. The arrows indicate the sites of in vivo cleavage by deubiquitylating enzymes. (B and C) Turnover of the core proteins. After a 24-h transfection with each UPR construct, cells were treated with 50 μg of cycloheximide/ml in the presence or absence of 10 μM MG132 for the different time periods indicated. Cells were lysed at the different time points indicated, followed by evaluation via sodium dodecyl sulfate-polyacrylamide gel electrophoresis and Western blot analysis using antibodies against the core protein and HA. (D) Quantitation of the data shown in panels B and C. At each time point, the ratio of band intensity of the core protein relative to the reference DHFR-HA-Ub^{R48} was determined by densitometry and is plotted as a percentage of the ratio at time zero.

tion with UPR constructs, cells were treated with cycloheximide and the amounts of core proteins and DHFR-HA-Ub^{R48} at the indicated time points were determined by Western blot analysis using anticore and anti-HA antibodies. The mature form of the core protein, aa 1 to 173 (C173) (13, 20), and C152 were degraded with first-order kinetics (Fig. 2B and D). MG132 completely blocked the degradation of C173 and C152 (Fig. 2B), and C152K6-23R and C152KR were markedly stabilized (Fig. 2C). The half-lives of C173 and C152 were calculated to be 5 to 6 h, whereas those of C152K6-23R and C152KR were calculated to be 22 to 24 h (Fig. 2D), confirming that the Ub plays an important role in regulating degradation of the core protein. Nevertheless, these results also suggest possible involvement of the Ub-independent pathway in the turnover of the core protein, as C152KR is more destabilized than the reference protein (Fig. 2C and 2D).

We have shown that PA28γ specifically binds to the core protein and is involved in its degradation (16, 17). Recent studies demonstrated that PA28γ is responsible for Ub-independent degradation of the steroid receptor coactivator SRC-3 and cell cycle inhibitors such as p21 (3, 11, 12). Thus, we next investigated the possibility of PA28γ involvement in the degradation of either C152KR or C152. Since C152KR carries two amino acid substitutions in the PA28γ-binding region (aa 44 to 71) (17), we tested the influence of the mutations of C152KR on the interaction with PA28γ by use of a coimmunoprecipi-

tation assay. When Flag-tagged PA28γ (F-PA28γ) was expressed in cells along with C152 or C152KR, F-PA28γ precipitated along with both C152 and C152KR, indicating that PA28γ interacts with both core proteins (Fig. 3A). Figure 3B reveals the effect of exogenous expression of F-PA28γ on the steady-state levels of C152 and C152KR. Consistent with previous data (17), the expression level of C152 was decreased to a nearly undetectable level in the presence of PA28γ (Fig. 3B, lanes 1 and 3). Interestingly, exogenous expression of PA28γ led to a marked reduction in the amount of C152KR expressed (Fig. 3B, lanes 5 and 7). Treatment with MG132 increased the steady-state level of the C152KR in the presence of F-PA28γ as well as the level of C152 (Fig. 3B, lanes 4 and 8).

We further investigated whether PA28γ affects the turnover of Lys-less core protein through time course experiments. C152KR was rapidly destabilized and almost completely degraded in a 3-h chase experiment using cells overexpressing F-PA28γ (Fig. 3C, left panels). A similar result was obtained using an analogous Lys-less mutant of the full-length core protein C191KR (Fig. 3C, right panels), thus demonstrating that the Lys-less core protein undergoes proteasomal degradation in a PA28γ-dependent manner. These results suggest that PA28γ may play a role in accelerating the turnover of the HCV core protein that is independent of ubiquitylation.

Finally, we examined gain- and loss-of-function of PA28γ with respect to degradation of full-length wild-type (C191) and mutated (C191KR) core proteins in human hepatoma Huh-7 cells. As expected, exogenous expression of PA28γ or E6AP caused a decrease in the C191 steady-state levels (Fig. 4A). In contrast, the C191KR level was decreased with expression of PA28γ but not of E6AP. We further used RNA interference to inhibit expression of PA28γ or E6AP. An increase in the abundance of C191KR was observed with PA28γ small interfering RNA (siRNA) but not with E6AP siRNA (Fig. 4B). An increase in the C191 level caused by the activity of siRNA against PA28γ or E6AP was confirmed as well.

Taking these results together, we conclude that turnover of the core protein is regulated by both Ub-dependent and Ub-independent pathways and that PA28γ is possibly involved in Ub-independent proteasomal degradation of the core protein. PA28 is known to specifically bind and activate the 20S proteasome (19). Thus, PA28γ may function by facilitating the delivery of the core protein to the proteasome in a Ub-independent manner.

Accumulating evidence suggests the existence of proteasome-dependent but Ub-independent pathways for protein degradation, and several important molecules, such as p53, p73, Rb, SRC-3, and the hepatitis B virus X protein, have two distinct degradation pathways that function in a Ub-dependent and Ub-independent manner (1, 2, 6, 7, 14, 21, 27). Recently, critical roles for PA28γ in the Ub-independent pathway have been demonstrated; SRC-3 and p21 can be recognized by the 20S proteasome independently of ubiquitylation through their interaction with PA28γ (3, 11, 12). It has also been reported that phosphorylation-dependent ubiquitylation mediated by GSK3 and SCF is important for SRC-3 turnover (26). Nevertheless, the precise mechanisms underlying turnover of most of the proteasome substrates that are regulated in both Ub-dependent and Ub-independent manners are not well understood. To our knowledge, the HCV core protein is the first

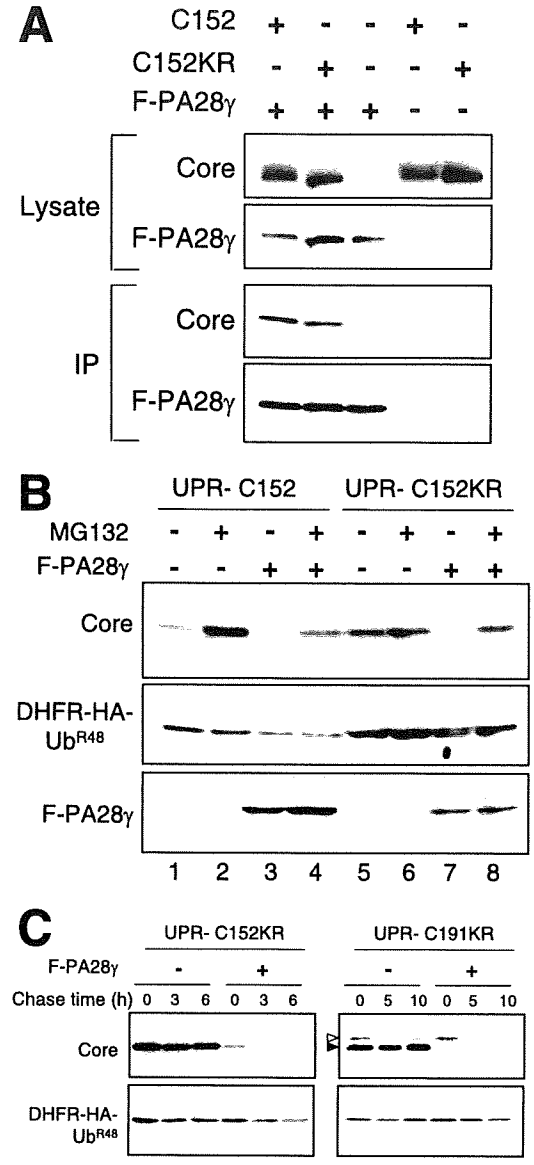

FIG. 3. PA28γ-dependent degradation of the core protein. (A) Interaction of the core protein with PA28γ. Cells were cotransfected with the wild-type (C152) or Lys-less (C152KR) core expression plasmid in the presence of a Flag-PA28γ (F-PA28γ) expression plasmid or an empty vector. The transfected cells were treated with MG132. After 48 h, the cell lysates were immunoprecipitated with anti-Flag antibody and visualized by Western blotting with anticore antibodies. Western blot analysis of whole cell lysates was also performed. (B) Degradation of the wild-type and Lys-less core proteins via the PA28γ-dependent pathway. Cells were transfected with the UPR construct with or without F-PA28γ. In some cases, cells were treated with 10 μM MG132 for 14 h before harvesting. Western blot analysis was performed using anticore, anti-HA, and anti-Flag antibodies. (C) After 24 h of transfection with UPR-C152KR and UPR-C191KR with or without F-PA28γ (an empty vector), cells were treated with 50 μg of cycloheximide/ml for different time periods as indicated (chase time). Western blot analysis was performed using anticore and anti-HA antibodies. The precursor core protein and the core that was processed, presumably by signal peptide peptidase, are denoted by open and closed triangles, respectively.

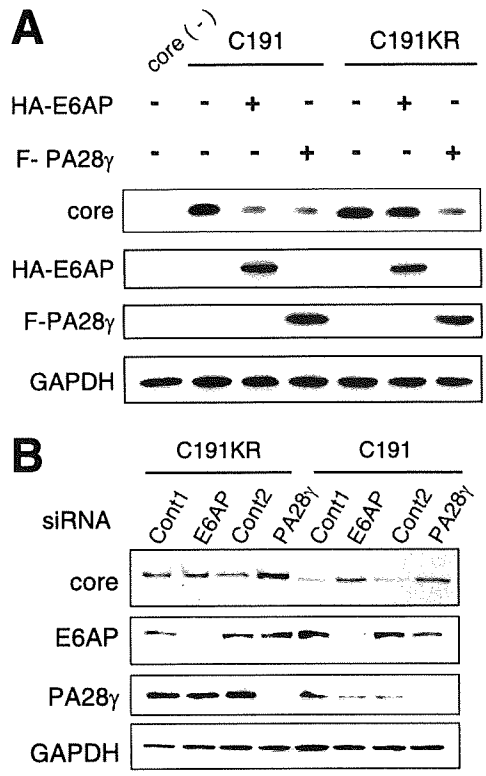

FIG. 4. Ub-dependent and Ub-independent degradation of the full-length core protein in hepatic cells. (A) Huh-7 cells were cotransfected with plasmids for the full-length core protein (C191) or its Lys-less mutant (C191KR) in the presence of F-PA28γ or HA-tagged-E6AP expression plasmid (HA-E6AP). After 48 h, cells were lysed and Western blot analysis was performed using anticore, anti-HA, anti-Flag, or anti-GAPDH. (B) Huh-7 cells were cotransfected with core expression plasmids along with siRNA against PA28γ or E6AP or with negative control siRNA. Cells were harvested 72 h after transfection and subjected to Western blot analysis.

viral protein studied that has led to identification of key cellular factors responsible for proteasomal degradation via dual distinct mechanisms. Although the question remains whether there is a physiological significance of the Ub-dependent and Ub-independent degradation of the core protein, it is reasonable to consider that tight control over cellular levels of the core protein, which is multifunctional and essential for viral replication, maturation, and pathogenesis, may play an important role in representing the potential for its functional activity.

This work was supported by a grant-in-aid for Scientific Research from the Japan Society for the Promotion of Science, from the Ministry of Health, Labor and Welfare of Japan, and from the Ministry of Education, Culture, Sports, Science and Technology, by Research on Health Sciences focusing on Drug Innovation from the Japan Health Sciences Foundation, Japan, and by the Program for Promotion of Fundamental Studies in Health Sciences of the National Institute of Biomedical Innovation of Japan.

REFERENCES

1. **Asher, G., J. Lotem, L. Sachs, C. Kahana, and Y. Shaul.** 2002. Mdm-2 and ubiquitin-independent p53 proteasomal degradation regulated by NQO1. Proc. Natl. Acad. Sci. USA **99**:13125–13130.
2. **Asher, G., P. Tsvetkov, C. Kahana, and Y. Shaul.** 2005. A mechanism of ubiquitin-independent proteasomal degradation of the tumor suppressors p53 and p73. Genes Dev. **19**:316–321.
3. **Chen, X., L. F. Barton, Y. Chi, B. E. Clurman, and J. M. Roberts.** 2007. Ubiquitin-independent degradation of cell-cycle inhibitors by the REGγ proteasome. Mol. Cell **26**:843–852.
4. **Ciechanover, A.** 1998. The ubiquitin-proteasome pathway: on protein death and cell life. EMBO J. **17**:7151–7160.
5. **Hershko, A., A. Ciechanover, and A. Varshavsky.** 2000. The ubiquitin system. Nat. Med. **6**:1073–1081.
6. **Jariel-Encontre, I., M. Pariat, F. Martin, S. Carillo, C. Salvat, and M. Piechaczyk.** 1995. Ubiquitinylation is not an absolute requirement for degradation of c-Jun protein by the 26 S proteasome. J. Biol. Chem. **270**:11623–11627.
7. **Jin, Y., H. Lee, S. X. Zeng, M. S. Dai, and H. Lu.** 2003. MDM2 promotes p21waf1/cip1 proteasomal turnover independently of ubiquitylation. EMBO J. **22**:6365–6377.
8. **Ju, D., and Y. Xie.** 2006. Identification of the preferential ubiquitination site and ubiquitin-dependent degradation signal of Rpn4. J. Biol. Chem. **281**: 10657–10662.
9. **Lai, M. M. C., and C. F. Ware.** 1999. Hepatitis C virus core protein: possible roles in viral pathogenesis. Springer, Berlin, Germany.
10. **Lévy, F., N. Johnsson, T. Rumenapf, and A. Varshavsky.** 1996. Using ubiquitin to follow the metabolic fate of a protein. Proc. Natl. Acad. Sci. USA **93**:4907–4912.
11. **Li, X., L. Amazit, W. Long, D. M. Lonard, J. J. Monaco, and B. W. O'Malley.** 2007. Ubiquitin- and ATP-independent proteolytic turnover of p21 by the REGγ-proteasome pathway. Mol. Cell **26**:831–842.
12. **Li, X., D. M. Lonard, S. Y. Jung, A. Malovannaya, Q. Feng, J. Qin, S. Y. Tsai, M. J. Tsai, and B. W. O'Malley.** 2006. The SRC-3/AIB1 coactivator is degraded in a ubiquitin- and ATP-independent manner by the REGγ proteasome. Cell **124**:381–392.
13. **Liu, Q., C. Tackney, R. A. Bhat, A. M. Prince, and P. Zhang.** 1997. Regulated processing of hepatitis C virus core protein is linked to subcellular localization. J. Virol. **71**:657–662.
14. **Lonard, D. M., Z. Nawaz, C. L. Smith, and B. W. O'Malley.** 2000. The 26S proteasome is required for estrogen receptor-α and coactivator turnover and for efficient estrogen receptor-α transactivation. Mol. Cell **5**:939–948.
15. **Moradpour, D., F. Penin, and C. M. Rice.** 2007. Replication of hepatitis C virus. Nat. Rev. Microbiol. **5**:453–463.
16. **Moriishi, K., R. Mochizuki, K. Moriya, H. Miyamoto, Y. Mori, T. Abe, S. Murata, K. Tanaka, T. Miyamura, T. Suzuki, K. Koike, and Y. Matsuura.** 2007. Critical role of PA28γ in hepatitis C virus-associated steatogenesis and hepatocarcinogenesis. Proc. Natl. Acad. Sci. USA **104**:1661–1666.
17. **Moriishi, K., T. Okabayashi, K. Nakai, K. Moriya, K. Koike, S. Murata, T. Chiba, K. Tanaka, R. Suzuki, T. Suzuki, T. Miyamura, and Y. Matsuura.** 2003. Proteasome activator PA28γ-dependent nuclear retention and degradation of hepatitis C virus core protein. J. Virol. **77**:10237–10249.
18. **Niwa, H., K. Yamamura, and J. Miyazaki.** 1991. Efficient selection for high-expression transfectants with a novel eukaryotic vector. Gene **108**:193–199.
19. **Realini, C., C. C. Jensen, Z. Zhang, S. C. Johnston, J. R. Knowlton, C. P. Hill, and M. Rechsteiner.** 1997. Characterization of recombinant REGα, REGβ, and REGγ proteasome activators. J. Biol. Chem. **272**:25483–25492.
20. **Santolini, E., G. Migliaccio, and N. La Monica.** 1994. Biosynthesis and biochemical properties of the hepatitis C virus core protein. J. Virol. **68**: 3631–3641.
21. **Sheaff, R. J., J. D. Singer, J. Swanger, M. Smitherman, J. M. Roberts, and B. E. Clurman.** 2000. Proteasomal turnover of p21Cip1 does not require p21Cip1 ubiquitination. Mol. Cell **5**:403–410.
22. **Shirakura, M., K. Murakami, T. Ichimura, R. Suzuki, T. Shimoji, K. Fukuda, K. Abe, S. Sato, M. Fukasawa, Y. Yamakawa, M. Nishijima, K. Moriishi, Y. Matsuura, T. Wakita, T. Suzuki, P. M. Howley, T. Miyamura, and I. Shoji.** 2007. E6AP ubiquitin ligase mediates ubiquitylation and degradation of hepatitis C virus core protein. J. Virol. **81**:1174–1185.
23. **Suzuki, R., K. Tamura, J. Li, K. Ishii, Y. Matsuura, T. Miyamura, and T. Suzuki.** 2001. Ubiquitin-mediated degradation of hepatitis C virus core protein is regulated by processing at its carboxyl terminus. Virology **280**:301–309.
24. **Suzuki, T., and A. Varshavsky.** 1999. Degradation signals in the lysine-asparagine sequence space. EMBO J. **18**:6017–6026.
25. **Treier, M., L. M. Staszewski, and D. Bohmann.** 1994. Ubiquitin-dependent c-Jun degradation in vivo is mediated by the δ domain. Cell **78**:787–798.
26. **Wu, R. C., Q. Feng, D. M. Lonard, and B. W. O'Malley.** 2007. SRC-3 coactivator functional lifetime is regulated by a phospho-dependent ubiquitin time clock. Cell **129**:1125–1140.
27. **Zhang, Z., and R. Zhang.** 2008. Proteasome activator PA28γ regulates p53 by enhancing its MDM2-mediated degradation. EMBO J. **27**:852–864.

THE JOURNAL OF BIOLOGICAL CHEMISTRY VOL. 284, NO. 8, pp. 5067–5076, February 20, 2009

Rho-kinase Contributes to Sustained RhoA Activation through Phosphorylation of p190A RhoGAP*[S]

Received for publication, September 4, 2008, and in revised form, December 4, 2008 Published, JBC Papers in Press, December 22, 2008, DOI 10.1074/jbc.M806853200

Kazutaka Mori[‡§1], Mutsuki Amano[‡1], Mikito Takefuji[‡§], Katsuhiro Kato[‡§], Yasuhiro Morita[‡§], Tomoki Nishioka[‡¶], Yoshiharu Matsuura[‖], Toyoaki Murohara[§], and Kozo Kaibuchi[‡2]

From the Departments of [‡] Cell Pharmacology, and [§] Cardiology, Graduate School of Medicine, Nagoya University, 65 Tsurumai, Showa-ku, Nagoya 466-8550, the [¶]Department of Forensic Medicine and Human Genetics, Kurume University School of Medicine, Kurume 830-0011, and the [‖]Department of Molecular Virology, Research Institute for Microbial Diseases, Osaka University, Osaka 565-0871, Japan

RhoA is transiently activated by specific extracellular signals such as endothelin-1 (ET-1) in vascular smooth muscle cells. RhoGAP negatively regulates RhoA activity: thus, RhoA becomes the GDP-bound inactive form afterward. Sustained activation of RhoA is induced with high doses of the extracellular signals and is implicated in certain diseases such as vasospasms. However, it remains largely unknown how prolonged activation of RhoA is induced. Here we show that Rho-kinase, an effector of RhoA, phosphorylated p190A RhoGAP at Ser^{1150} and attenuated p190A RhoGAP activity in COS7 cells. Binding of Rnd to p190A RhoGAP is thought to enhance its activation. Phosphorylation of p190A RhoGAP by Rho-kinase impaired Rnd binding. Stimulation of vascular smooth muscle cells with a high dose of ET-1 provoked sustained RhoA activation and p190A RhoGAP phosphorylation, both of which were prohibited by a Rho-kinase inhibitor. The phosphomimic mutation of p190A RhoGAP weakened Rnd binding and RhoGAP activities. Taken together, these results suggest that ET-1 induces Rho-kinase activation and subsequent phosphorylation of p190A RhoGAP, leading to prolonged RhoA activation.

RhoA small GTPase is the molecular switch for various extracellular signals and is implicated in a variety of biological functions, including cell contraction, cell migration, cell adhesion, cell cycle progression, and gene expression (1, 2). RhoA regulates these functions through its specific effectors such as Rho-kinase/ROCK/ROK and mDia (2). We previously found that Rho-kinase phosphorylates myosin phosphatase target protein 1 (MYPT1)[3] of myosin phosphatase and thereby inactivates its phosphatase activity, resulting in an increase in the phosphorylation of myosin light chain followed by smooth muscle contraction (3–5). Rho-kinase increases the agonist-induced Ca^{2+} sensitivity and contributes to sustained contraction of smooth muscle (6).

RhoA cycles between the GTP-bound active and GDP-bound inactive conformations. This cycle is under the direct control of three groups of regulatory proteins: the guanine nucleotide exchange factors (GEFs), which catalyze the exchange of GDP for GTP to activate RhoA; GTPase-activating proteins (GAPs), which enhance the intrinsic GTPase activity of RhoA to promote hydrolysis of GTP to GDP to inactivate RhoA; and the guanine nucleotide dissociation inhibitors, which sequester the GDP-bound RhoA and may also regulate its intracellular localization (1, 2).

The typical RhoGEFs contain a catalytic Dbl homology domain and an adjacent pleckstrin homology domain. This Dbl homology-associated pleckstrin homology domain interacts with phospholipids, which may localize GEFs to the plasma membrane and activate GEF activity (7, 8). RhoA activation is often mediated by G protein-coupled receptors. Three RhoGEFs, which contain the regulator of G protein-signaling domains, including leukemia-associated RhoGEF, PDZ-RhoGEF, and p115RhoGEF, directly link between $G\alpha_{12}/G\alpha_{13}$ and RhoA (9–11). $G\alpha_{12}$ and $G\alpha_{13}$ specifically interact with the regulator of G protein-signaling domains of these RhoGEFs and positively regulate their GEF activity (12). The typical RhoGAPs have a catalytic domain and various domains for protein-protein interaction. Recent studies suggest that RhoGAPs are regulated by various mechanisms, including protein-protein interaction, phospholipid interaction, phosphorylation, subcellular translocation, and proteolytic degradation (13, 14). However, the precise mechanisms that regulate RhoGAP activity remain elusive in many cases.

When the smooth muscle cells are stimulated with agonists such as ET-1, RhoA is transiently activated presumably through RhoA-specific GEFs such as leukemia-associated RhoGEF and inactivated later (11, 15). The RhoA-specific GAP appears to be responsible for RhoA inactivation under physiological conditions (16). Sustained RhoA/Rho-kinase activation occurs with

* This work was supported by grants-in-aid for creative science research and a grant-in-aid for scientific research (S: 20227006; C: 20590308), by the Global Centers of Excellence Program from the Ministry of Education, Culture, Sports, Science, and Technology of Japan, and by the Program for Promotion of Fundamental Studies in Health Sciences of the National Institute of Biomedical Innovation (Grant 02-3). The costs of publication of this article were defrayed in part by the payment of page charges. This article must therefore be hereby marked "*advertisement*" in accordance with 18 U.S.C. Section 1734 solely to indicate this fact.

[S] The on-line version of this article (available at http://www.jbc.org) contains supplemental Figs. S1–S5.

[1] Both authors contributed equally to this work.

[2] To whom correspondence should be addressed. Tel.: 81-52-744-2074; Fax: 81-52-744-2083; E-mail: kaibuchi@med.nagoya-u.ac.jp.

[3] The abbreviations used are: MYPT1, myosin phosphatase target protein-1; ET-1, endothelin-1; GEF, guanine nucleotide exchange factor; GAP, GTPase-activating protein; FL, full length; RBD, Rho-binding domain; WT, wild-type; GFP, green fluorescent protein; GST, glutathione S-transferase; aa, amino acid(s); HA, hemagglutinin; Ab, antibody.

high doses of ET-1 (17). Prolonged activation of RhoA/Rho-kinase is implicated in the pathogenesis of certain vascular diseases, including subarachnoid hemorrhage-induced cerebral vasospasm, coronary vasospasm, essential hypertension, and pulmonary hypertension (18, 19). For example, RhoA activity is higher in aortic smooth muscle cells derived from the stroke-prone spontaneously hypertensive rat than from the wild-type rat, although the expression levels of RhoA are not different between mutant and wild-type rats (20). Rho-kinase activity is up-regulated, and phosphorylation levels of MYPT1 are increased in the coronary spastic lesion in a porcine swine model (21). Subarachnoid hemorrhage induces sustained Rho-kinase activation in the canine basilar artery and subsequent cerebral vasospasm (22). Chronic hypoxia-induced pulmonary hypertension in rats is associated with an increase of RhoA activity in pulmonary artery (23). However, it remains largely unknown how prolonged activation of RhoA is induced.

In light of these observations, we hypothesized that highly activated RhoA/Rho-kinase can inhibit Rho-specific GAP and lead to sustained RhoA activation. Here we show that Rho-kinase phosphorylated p190A RhoGAP, the best characterized RhoA-specific GAP, at Ser^{1150} *in vitro* and *in vivo*. Phosphorylation of p190A RhoGAP by Rho-kinase appeared to attenuate its GAP activity.

EXPERIMENTAL PROCEDURES

Materials and Chemicals—The cDNA-encoding human p190A RhoGAP (KIAA1722, p190A) was obtained from the Kazusa DNA Research Institute (Chiba, Japan). Monoclonal anti-GFP antibody was purchased from Roche Diagnostics (Mannheim, Germany). Polyclonal anti-GFP antibody was from MBL (Nagoya, Japan). Monoclonal anti-p190A RhoGAP antibodies were from BD Biosciences Pharmingen (San Diego, CA) and Upstate Biotechnology (Lake Placid, NY). Monoclonal anti-RhoA antibody was from Santa Cruz Biotechnology, Inc. (Santa Cruz, CA). Monoclonal anti-HA antibody (12CA5) was from Boehringer (Ingelheim, Germany). Polyclonal anti-MYPT1-pT853 antibody was from Upstate Biotechnology. Polyclonal anti-total MYPT1 antibody was generated as previously described (24). A rabbit polyclonal antibody against p190A RhoGAP phosphorylated at Ser^{1150} was produced against the phosphopeptide Cys-Arg^{1145}-Gly-Arg-Lys-Val-phospho-Ser^{1150}-Ile-Val-Ser-Lys-Pro^{1155} by Biologica Co. (Nagoya, Japan). Y-27632, a Rho-kinase-specific inhibitor, was provided by Mitsubishi Pharma Co. (Osaka, Japan). ET-1, BQ-123, and BQ-788 were from Sigma. Other materials and chemicals were obtained from commercial sources.

Plasmid Constructs and Protein Purification—p190A RhoGAP fragments were amplified by PCR and subcloned into pGEX-2T (GE Healthcare, Princeton, NJ) or pEGFP-C1 (Clontech Laboratories, Mountain View, CA) plasmids, respectively. The cDNAs of p190A RhoGAP-4-S1150A, p190A RhoGAP-4-S1150A/T1173A/S1174A (p190A RhoGAP-4-AAA), p190A RhoGAP-4-S1150E/T1173E/S1174E (p190A RhoGAP-4-EEE), p190A RhoGAP-5-T1226A/S1236A (p190A RhoGAP-5-AA), p190A RhoGAP-5-T1226A/T1241A, p190A RhoGAP-full-length-S1150A (p190A RhoGAP-FL-S1150A), and p190A RhoGAP-FL-S1150E/T1173E/S1174E/T1226E/S1236E (p190A RhoGAP-FL-5E), in which Ala or Glu was substituted for Ser^{1150}, Thr^{1173}, Ser^{1174}, Thr^{1226}, Ser^{1236}, and/or Thr^{1241} were generated by site-directed mutagenesis. Rnd1 was isolated by PCR from a cDNA library and subcloned into pEF-BOS-HA plasmid. All fragments were confirmed by DNA sequencing. Glutathione *S*-transferase (GST) fusion proteins were produced in *Escherichia coli* BL21(DE3) and purified on glutathione-Sepharose 4B beads (GE Healthcare). GST-Rho-kinase-CAT (aa 6–553), a constitutively active form of Rho-kinase, and GST-p190A RhoGAP-4 + 5 (aa 953–1499) were produced in Sf9 cells with a baculovirus system and purified on glutathione-Sepharose 4B beads.

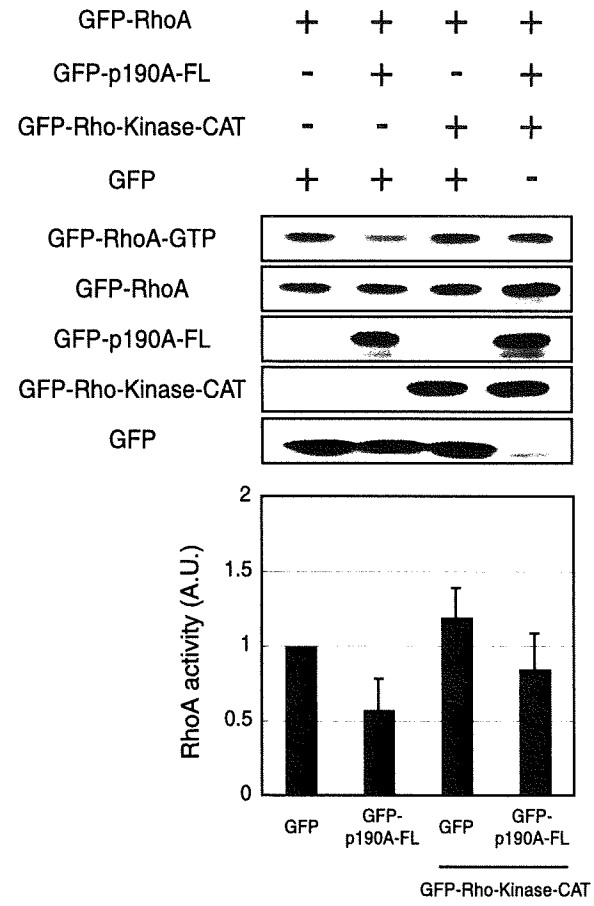

FIGURE 1. **Counteraction of p190A RhoGAP function by Rho-kinase in intact cells.** COS7 cells transfected with the indicated constructs were lysed with lysis buffer, and the lysates were incubated with GST-Rhotekin-RBD to precipitate the GTP-bound active form of RhoA. The eluates were analyzed by immunoblotting with anti-GFP Ab (*top*). The ratio of GFP-RhoA-GTP to total GFP-RhoA is shown (*bottom*). Data represent the means ± S.E. of four independent experiments.

Phosphorylation Assay—The phosphorylation assay was performed as previously described (25). In brief, the kinase reaction of Rho-kinase for p190A RhoGAP was carried out in 50 μl of the reaction mixture (50 mM Tris/HCl, pH 7.5, 1 mM EDTA, 1 mM EGTA, 1 mM dithiothreitol, 5 mM $MgCl_2$) containing 100 μM [γ-^{32}P]ATP (1–20 GBq/mmol), purified GST-Rho-kinase-CAT (0.001–0.1 μM), and 1 μM purified GST-p190A RhoGAP fragments. After incubation for 10 min at 30 °C, the reaction mixtures were boiled in SDS sample

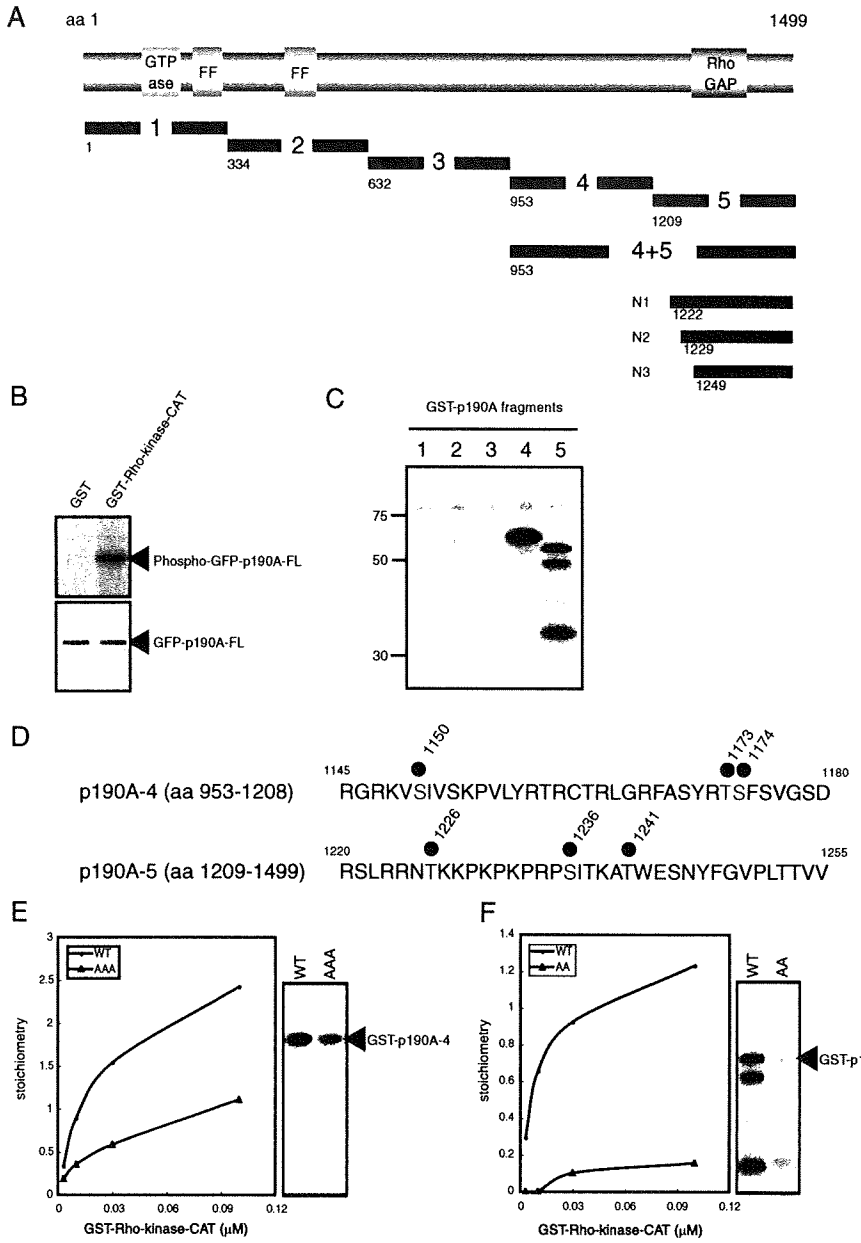

FIGURE 2. **Determination of phosphorylation sites of p190A RhoGAP by Rho-kinase.** *A*, schematic representation of domain structure and deletion constructs of p190A RhoGAP. *B*, immunoprecipitated GFP-p190A RhoGAP-FL from COS7 cell lysates was incubated with GST (*left*) or GST-Rho-kinase-CAT (*right*) and 100 μM [γ-^{32}P]ATP for 30 min at 30 °C. The reaction mixtures were subjected to SDS-PAGE and GFP-p190A RhoGAP was visualized by silver staining (*lower panel*). Phosphorylated proteins were imaged by autoradiography (*upper panel*). *C*, mapping of the region in p190A RhoGAP phosphorylated by Rho-kinase. The indicated GST-p190A RhoGAP fragments were phosphorylated by GST-Rho-kinase-CAT. The phosphorylated proteins were imaged by autoradiography. *D*, the phosphorylation sites of p190A RhoGAP are represented. Phosphorylated serine and threonine are in *red*. *E*, phosphorylation of GST-p190A RhoGAP-4-S1150A/T1173A/S1174A (*AAA*) by GST-Rho-kinase-CAT. *F*, phosphorylation of GST-p190A RhoGAP-5-T1226A/S1236A (*AA*) by GST-Rho-kinase-CAT. These results are representative of three independent experiments.

buffer and subjected to SDS-PAGE. The radiolabeled bands were visualized and estimated by an image analyzer (BAS2000, Fuji, Tokyo, Japan).

GAP Assay—The RhoA GAP assay was performed as previously described (26). Briefly, recombinant GST-RhoA was preloaded with 1 μM [γ-^{32}P]GTP (222 TBq/mmol, PerkinElmer Life Sciences) in 25 μl of buffer containing 50 mM HEPES, pH 7.4, 50 mM NaCl, 0.1 mM dithiothreitol, 0.1 mM EGTA, 5 mM EDTA, and 1 mg/ml bovine serum albumin for 10 min at 30 °C before the addition of $MgCl_2$ to a final concentration of 10 mM. An aliquot of [γ-^{32}P]GTP-loaded GST-RhoA was mixed with the GAP assay buffer, which contained 25 mM HEPES, pH 7.5, 50 mM NaCl, 1 mM $MgCl_2$, 0.1 mM dithiothreitol, 0.1 mM GTP, and 1 mg/ml bovine serum albumin in the presence of nonphosphorylated GST-p190A RhoGAP-4 + 5 or phosphorylated GST-p190A RhoGAP-4 + 5. The reaction was performed for 5 min at 30 °C and terminated by rapid addition of 5 ml of ice-cold buffer containing 50 mM HEPES, pH 7.5, 50 mM NaCl, and 1 mM $MgCl_2$. The samples were then immediately deposited onto nitrocellulose filters. The radioactivity retained on the filter was then subjected to quantitative analysis by scintillation counting. RhoGAP activity was detected as the remainder of [γ-^{32}P]GTP bound to GST-RhoA.

GTP-Rho Pulldown Assay—The activity of RhoA was determined by pulldown assay with the GST-Rho-binding domain of Rhotekin (GST-Rhotekin-RBD) as previously described (27). Briefly, the cells were washed with ice-cold phosphate-buffered saline and lysed in 500 μl of lysis buffer (50 mM Tris/HCl, pH 7.5, 1 mM EDTA, 10 mM $MgCl_2$, 500 mM NaCl, 0.5% Nonidet P-40, 0.1 mM (*p*-amidinophenyl)methanesulfonyl fluoride, 2.5 μg/ml aprotinin, 2.5 μg/ml leupeptin) containing 20 μg of GST-Rhotekin-RBD. The lysates were centrifuged at 20,000 × *g* for 3 min at 4 °C, and the supernatants were incubated with glutathione-Sepharose 4B beads for 30 min at 4 °C. The beads were washed with an excess of lysis buffer and then eluted with SDS-sample buffer. The eluates were subjected to SDS-PAGE, followed by immunoblot analysis with anti-GFP antibody or anti-RhoA antibody.

Rnd1-binding Assay—COS7 cells were transiently transfected with pEF-BOS-HA-Rnd1. The cells were washed with phosphate-buffered saline and lysed with lysis buffer (20 mM Tris/HCl, pH 7.5, 1 mM EDTA, 150 mM NaCl, 1 mM dithiothre-

itol, 1% Nonidet P-40, 0.2 μM Calyculin A, 1 mM sodium orthovanadate, 0.1 mM (*p*-amidinophenyl)methanesulfonyl fluoride, 2.5 μg/ml aprotinin, 2.5 μg/ml leupeptin). The lysates were centrifuged at 20,000 × *g* for 20 min at 4 °C, and the supernatants were incubated with glutathione-Sepharose 4B beads coated with 200 or 400 pmol of GST, 100 or 200 pmol of phosphorylated GST-p190A RhoGAP-4, and 100 or 200 pmol of nonphosphorylated GST-p190A RhoGAP-4 for 1 h at 4 °C. The beads were washed, and the eluates were subjected to SDS-PAGE, followed by immunoblot analysis with anti-HA antibody.

Cell Culture and Agonist Stimulation—Human aortic smooth muscle cells were obtained from Takara Bio Inc. (Shiga, Japan) and cultured in Dulbecco's modified Eagle's medium containing 10% fetal bovine serum, 100 units/ml penicillin, and 100 μg/ml streptomycin. Human aortic smooth muscle cells at the sixth passage were transfected with GFP-p190A RhoGAP-FL by using the Nucleofector system (Amaxa, Cologne, Germany). 24 h after transfection, the cells were starved for serum of 8 h and then stimulated with 1 μM ET-1. For the experiments with inhibitors, the cells were pretreated with inhibitors 30 min before ET-1 stimulation.

Measurement of Cell Size—To measure the cell size, human aortic smooth muscle cells were transfected with plasmids by using the Nucleofector system and then seeded on glass coverslips coated with fibronectin (BD Biosciences Pharmingen). 24 h after transfection, the cells were fixed with 3.0% formaldehyde in phosphate-buffered saline for 10 min and then treated with phosphate-buffered saline containing 0.1% Triton X-100 for 10 min. The cell area was measured with a laser scanning confocal microscope (model LSM510, Carl Zeiss, Oberkochene, Germany).

RESULTS

Counteraction of p190A RhoGAP Function by Rho-kinase—p190A and p190B RhoGAPs are ubiquitously expressed in various tissues and display GAP activity exclusively toward RhoA *in vivo* (28, 29). p190RhoGAP activity accounts for ~60% of the total RhoGAP activity detected in whole cell extracts in fibroblasts (30). Inhibition of p190RhoGAP activity is sufficient to promote RhoA activation in fibroblasts (30). Knockdown of p190A RhoGAP activity using siRNA increases RhoA activity in spreading microvascular endothelial cells (31). Thus, p190RhoGAP appears to account for the majority of RhoGAP activity.

Hence, we first examined whether Rho-kinase affects the p190A RhoGAP function in intact cells. GFP-RhoA was transfected into COS7 cells, and the amount of the GTP-bound form of GFP-RhoA was monitored by pulldown assay (Fig. 1). The expression of GFP-p190A RhoGAP-FL decreased the amount of GTP-bound GFP-RhoA in COS7 cells, suggesting that GFP-p190A RhoGAP-FL acts as RhoAGAP. The amount of GTP-bound GFP-RhoA was greater in the cells expressing GFP-p190A RhoGAP-FL and GFP-Rho-kinase-CAT than that in the cells expressing GFP-p190A RhoGAP-FL alone. This result suggests that Rho-kinase counteracts the GAP activity of p190A RhoGAP in COS7 cells.

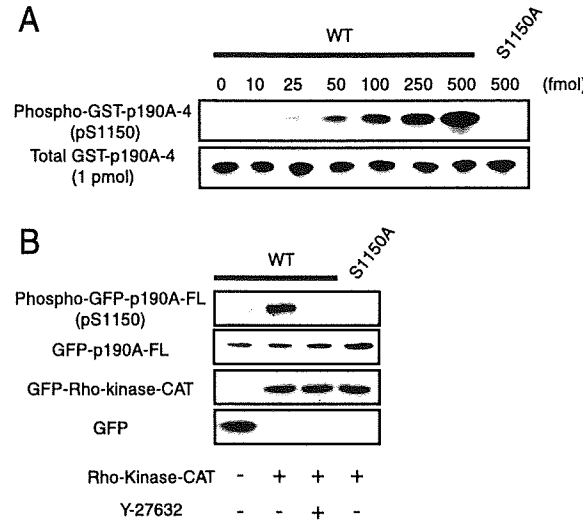

FIGURE 3. **Rho-kinase-dependent phosphorylation of p190A RhoGAP at Ser^{1150}.** *A*, specificity of the purified antibody against p190A RhoGAP phosphorylated at Ser^{1150}. One picomole of GST-p190A RhoGAP-4 containing the indicated amounts of phosphorylated GST-p190A RhoGAP-4-WT or -S1150A was subjected to SDS-PAGE, followed by immunoblot analysis with anti-p190A RhoGAP-pS1150 Ab (*upper panel*) or anti-GST Ab (*lower panel*). *B*, phosphorylation of p190A RhoGAP by Rho-kinase in intact cells. GFP-p190A RhoGAP-FL-WT or -S1150A was transiently transfected together with either GFP-Rho-kinase-CAT or GFP into COS7 cells as indicated. The transfected cells were treated with 20 μM Y-27632 or DMSO for the last 30 min of transfection. The cell lysates were analyzed by immunoblotting with anti-p190A RhoGAP-pS1150 Ab or anti-GFP Ab. These results are representative of three independent experiments.

In Vitro Phosphorylation of p190A RhoGAP by Rho-kinase—We then examined whether p190A RhoGAP is phosphorylated by Rho-kinase *in vitro*. To make a full length of p190A RhoGAP, we transiently transfected COS7 cells with GFP-p190A RhoGAP-FL, and immunoprecipitated GFP-p190A RhoGAP-FL from cell lysates with a polyclonal anti-GFP antibody. The immunoprecipitated GFP-p190A RhoGAP-FL was effectively phosphorylated by GST-Rho-kinase-CAT *in vitro* (Fig. 2*B*). We also found that Rho-kinase phosphorylated p190B RhoGAP (data not shown).

To determine the phosphorylation sites of p190A RhoGAP by Rho-kinase, p190A RhoGAP was divided into five fragments, including GST-p190A RhoGAP-1 (aa 1–333), p190A RhoGAP-2 (aa 334–637), p190A RhoGAP-3 (aa 632–952), p190A RhoGAP-4 (aa 953–1208), and p190A RhoGAP-5 (aa 1209–1499) (Fig. 2*A*). These fragments were produced from *E. coli* and then purified. GST-p190A RhoGAP-4 and p190A RhoGAP-5 were effectively phosphorylated by GST-Rho-kinase-CAT, whereas GST-p190A RhoGAP-1, GST-p190A RhoGAP-2, and GST-p190A RhoGAP-3 were not phosphorylated (Fig. 2*C*). To identify potential phosphorylation sites in p190A RhoGAP, liquid chromatography tandem mass spectrometry was performed and three potential phosphorylation sites in p190A RhoGAP-4 were identified, namely Ser^{1150}, Thr^{1173}, and Ser^{1174} (Fig. 2*D*). To determine the major phosphorylation sites, we substituted Ser^{1150}, Thr^{1173}, or Ser^{1174} with Ala to produce GST-p190A RhoGAP-4-S1150A, GST-p190A RhoGAP-4-T1173A, and GST-p190A RhoGAP-4-S1174A. However, the single Ala substitution did not affect the

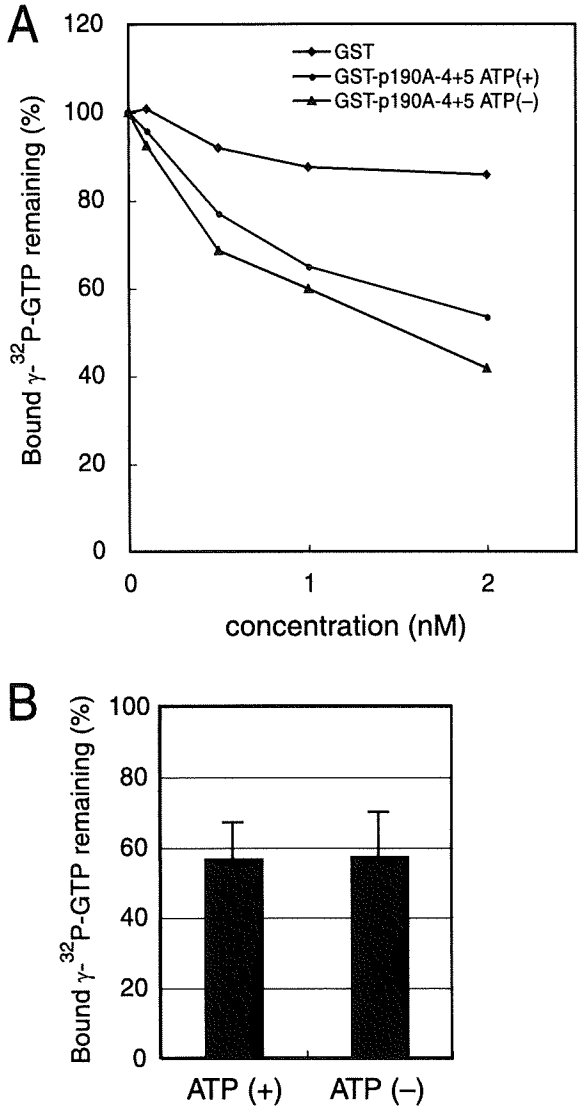

FIGURE 4. **Effect of phosphorylation of p190A RhoGAP by Rho-kinase on its GAP activity *in vitro*.** *A*, GST-p190A RhoGAP-4+5 was produced in Sf9 cells with a baculovirus system and purified on glutathione-Sepharose beads. Hydrolysis of GTP-bound GST-RhoA was monitored with GST (*squares*), nonphosphorylated GST-p190A RhoGAP-4+5 (*triangles*), or phosphorylated GST-p190A RhoGAP-4+5 (*circles*) for 5 min at 30 °C. The result is representative of three independent experiments. *B*, 1 μM [γ-^{32}P]GTP-bound GST-RhoA was incubated with 1 nM nonphosphorylated RhoGAP-4+5 or phosphorylated GST-p190A RhoGAP-4+5 for 5 min at 30 °C. Data are indicated as mean ± S.D. (n = 20, respectively, p = 0.82).

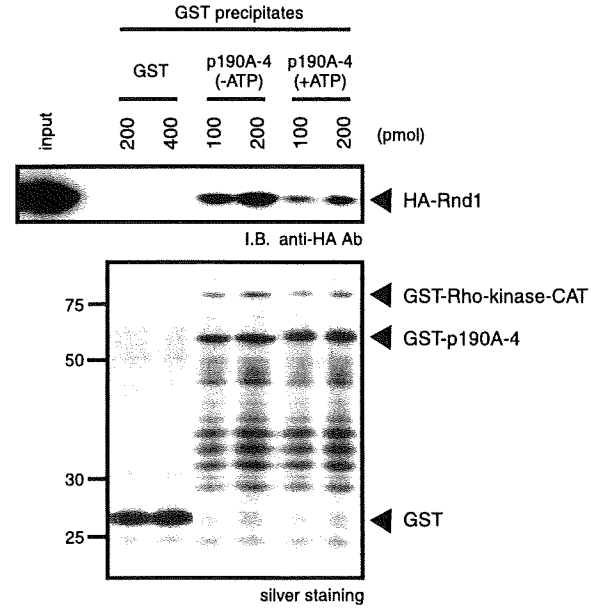

FIGURE 5. **Binding of p190A RhoGAP to Rnd1.** COS7 cells were transiently transfected with pEF-BOS-HA-Rnd1. The cell lysates were incubated with glutathione-Sepharose 4B beads coated with 200 or 400 pmol of GST, 100 or 200 pmol of phosphorylated GST-p190A RhoGAP-4, and 100 or 200 pmol of nonphosphorylated GST-p190A RhoGAP-4 for 1 h at 4 °C. The beads were washed, and the eluates were subjected to SDS-PAGE, followed by immunoblot analysis with anti-HA Ab. GST fusion proteins were visualized by silver staining. The result is representative of three independent experiments.

phosphorylation efficiency (data not shown). Then, Ser^{1150}, Thr^{1173}, and Ser^{1174} were simultaneously substituted with Ala to produce GST-p190A RhoGAP-4-S1150A/T1173A/S1174A (GST-p190A RhoGAP-4-AAA). The phosphorylation efficiency of GST-p190A RhoGAP-4-AAA was substantially reduced compared with the wild type (Fig. 2*E*), suggesting that at least two potential phosphorylation sites among these three sites are efficient phosphorylation sites.

The phosphorylation sites in p190A RhoGAP-5 were not identified by liquid chromatography tandem mass spectrometry. To identify potential phosphorylation sites in p190A RhoGAP-5, we produced the additional deletion mutants, including GST-p190A RhoGAP-ΔN1 (aa 1222–1499), p190A RhoGAP-ΔN2 (aa 1229–1499), and p190A RhoGAP-ΔN3 (aa 1249–1499) (Fig. 2*A*). GST-p190A RhoGAP-ΔN1 was highly phosphorylated and GST-p190A RhoGAP-ΔN2 was intermediately phosphorylated by GST-Rho-kinase-CAT, whereas GST-p190A RhoGAP-ΔN3 was not phosphorylated (supplemental Fig. S1*A*), suggesting that phosphorylation sites exist in aa 1222–1228 and aa 1229–1248. Because (R/K)*XX*(S/T) or (R/K)*X*(S/T) (X is any amino acid) is the consensus phosphorylation sequence by Rho-kinase, the potential phosphorylation sites in p190A-5 are Thr^{1226} in aa 1222–1228, and Ser^{1236} and Thr^{1241} in aa 1229–1248 (Fig. 2*D*), suggesting that Thr^{1226} is the putative major phosphorylation site. To determine the major phosphorylation sites in p190A RhoGAP-5, we produced GST-p190A RhoGAP-5-T1226A/S1236A (GST-p190A RhoGAP-5-AA) and GST-p190A RhoGAP-5-T1226A/T1241A. GST-p190A RhoGAP-5-AA was minimally phosphorylated by GST-Rho-kinase-CAT (Fig. 2*F*). The degree of phosphorylation of GST-p190A RhoGAP-5-T1226A/T1241A by GST-Rho-kinase-CAT was approximately half (supplemental Fig. S1*B*). Taken together, these results suggest that Rho-kinase phosphorylates p190A RhoGAP presumably at a minimum of five sites, including Ser^{1150}, Thr^{1173}, Ser^{1174}, Thr^{1226}, and Ser^{1236} *in vitro*.

In Vivo Phosphorylation of p190A RhoGAP by Rho-kinase—To examine the phosphorylation state of p190A RhoGAP by Rho-kinase *in vivo*, we prepared rabbit polyclonal antibodies that specifically recognize p190A RhoGAP phosphorylated at respective phosphorylation sites. Among them, the anti-p190A RhoGAP-pS1150 antibody specifically recognized GST-p190A

Phosphorylation of p190A RhoGAP by Rho-kinase

RhoGAP-4 phosphorylated by GST-Rho-kinase-CAT in a dose-dependent manner, but not phosphorylated GST-p190A RhoGAP-4-S1150A (Fig. 3*A*), indicating that the antibody specifically recognized GST-p190A RhoGAP-4 that was phosphorylated at Ser^{1150}. The anti-p190A RhoGAP-pT1173 and pS1174 antibodies only slightly recognized phosphorylated p190A RhoGAP, suggesting that Thr^{1173} and Ser^{1174} are not major phosphorylation sites. Alternatively, these antibodies did not work well on phosphorylated p190A RhoGAP, although they recognized the antigen phosphopeptides (data not shown). The anti-p190A RhoGAP-pT1226 and -pS1236 antibodies could recognize the phosphorylated p190A RhoGAP *in vitro* in a manner similar to that of anti-p190A RhoGAP-pS1150 antibody (data not shown).

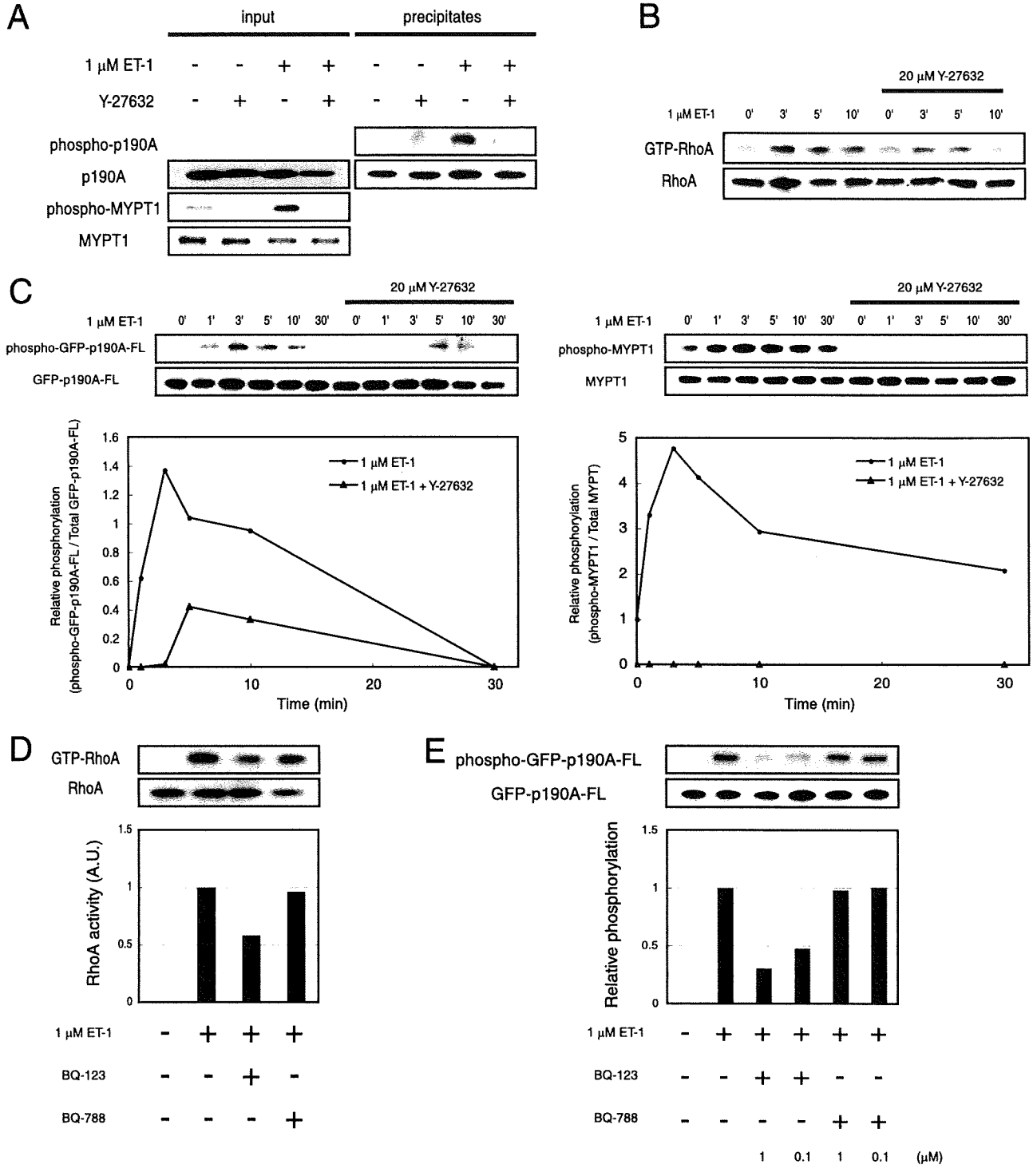

To examine whether Rho-kinase phosphorylates p190A RhoGAP in intact cells, GFP-p190A RhoGAP-FL was exogenously co-transfected with GFP-Rho-kinase-CAT into COS7 cells. Co-transfection of Rho-kinase-CAT resulted in an increase of phosphorylated GFP-p190A RhoGAP-FL at Ser^{1150} (Fig. 3*B*). Treatment of the cells with Y-27632 inhibited phosphorylation of GFP-p190A RhoGAP-FL by GFP-Rho-kinase-CAT. GFP-Rho-kinase-CAT failed to phosphorylate GFP-p190A RhoGAP-FL-S1150A. Under the same conditions, phosphorylation of endogenous p190A RhoGAP at Ser^{1150} was not detected, presumably because the expression level of p190A RhoGAP was low in COS7 cells. Taken together, these results indicate that Rho-kinase can phosphorylate p190A RhoGAP at Ser^{1150} in COS7 cells. Similarly, the immunoblot analysis, through the use of the anti-p190A RhoGAP-pT1226 and -pS1236 antibodies, revealed that Rho-kinase can phosphorylate p190A RhoGAP at Thr^{1226} and Ser^{1236} in COS7 cells (data not shown).

Effects of Phosphorylation of p190A RhoGAP by Rho-kinase on Its GAP Activity—Does phosphorylation of p190A RhoGAP by Rho-kinase affect p190A RhoGAP functions? To examine the effects of phosphorylation on the GAP activity of p190A RhoGAP, we tried to produce and purify the full length of p190A RhoGAP from *E. coli* and insect cells, but the procedure failed. We then prepared nonphosphorylated and phosphorylated GST-p190A RhoGAP-4+5, which includes the identified five phosphorylation sites and the RhoGAP catalytic domain, and performed an *in vitro* GAP assay. Hydrolysis of GTP-bound GST-RhoA was accelerated by using purified GST-p190A RhoGAP-4+5 in a dose-dependent and time-dependent manner (supplemental Fig. S2). The GAP activity of GFP-p190A RhoGAP-4+5 was not dramatically affected by phosphorylation (Fig. 4, *A* and *B*).

We here found that Rho-kinase appeared to inhibit the p190A RhoGAP activity in COS7 cells (Fig. 1). How does Rho-kinase regulate the GAP activity of p190A RhoGAP in intact cells? Small GTPase Rnd is a member of the distinct subgroup of the Rho family GTPases and regulates the organization of actin cytoskeleton (32). Expression of Rnd inhibits the formation of the stress fibers in response to lysophosphatidic acid stimulation in fibroblasts (33), suggesting that Rnd antagonizes the action of RhoA. Consistently, Rnd binds to p190A RhoGAP and increases its GAP activity toward GTP-bound RhoA, resulting in RhoA inactivation (34, 35). This observation prompted us to examine whether phosphorylation of p190A RhoGAP affects its interaction with Rnd1. HA-Rnd1 efficiently interacted with GST-p190A RhoGAP-4 in the pulldown assay, and phosphorylation of GST-p190A RhoGAP-4 by Rho-kinase attenuated its interaction with Rnd1 (Fig. 5). Thus, it is conceivable that Rho-kinase suppresses the GAP activity of p190A RhoGAP by inhibiting the interaction with Rnd1 through phosphorylation.

Phosphorylation of p190A RhoGAP in Cultured Vascular Smooth Muscle Cells—To understand the physiological functions of p190A RhoGAP, we confirmed the expression profile of p190A RhoGAP in various rat tissues and found that p190A RhoGAP was highly expressed in brain, lung, and aorta (supplemental Fig. S3*A*). We also found that p190A RhoGAP was highly expressed in primary human aortic smooth muscle and endothelial cells (supplemental Fig. S3*B*).

Then, we monitored phosphorylation of endogenous p190A RhoGAP in human aortic smooth muscle cells. The basal phosphorylation level of p190A RhoGAP at Ser^{1150} was not detected (Fig. 6*A*). ET-1 is known to activate the Rho/Rho-kinase pathway (17). Stimulation of smooth muscle cells by ET-1 induced phosphorylation of endogenous p190A RhoGAP at Ser^{1150} (Fig. 6*A*). Treatment of the cells with Y-27632 inhibited ET-1-induced phosphorylation of p190A RhoGAP. As a positive control, the MYPT1 phosphorylation level was monitored. Phosphorylation of MYPT1 at Thr^{853} decreases the activity of myosin phosphatase in vascular smooth muscle cells: this phosphorylation is used as an indicator of the activity of Rho-kinase (17). ET-1 induced phosphorylation of MYPT1 at Thr^{853}, whereas Y-27632 completely inhibited this phosphorylation. Taken together, these results suggest that ET-1 provoked phosphorylation of endogenous p190A RhoGAP at Ser^{1150} in a Rho-kinase dependent fashion in cultured vascular smooth muscle cells.

Of note, the immunoblot analysis using the anti-p190A RhoGAP-pT1226 and -pS1236 antibodies revealed that p190A RhoGAP was phosphorylated upon treatment with ET-1, but these phosphorylations were not dramatically inhibited by Y-27632, suggesting that these sites are not major phosphorylation sites by Rho-kinase in aortic smooth muscle cells (data not shown).

A high concentration of ET-1 has been shown to induce activation of Rho/Rho-kinase and subsequent MYPT1 phosphorylation, thereby resulting in the sustained contraction of vascular

FIGURE 6. **Phosphorylation of p190A RhoGAP by Rho-kinase in cultured vascular smooth muscle cells.** *A*, phosphorylation of endogenous p190A RhoGAP in cultured vascular smooth muscle cells. The cells were incubated with 20 μM Y-27632 or DMSO for 30 min, and then treated with 1 μM ET-1 for 3 min. Endogenous p190A RhoGAP was immunoprecipitated with anti-p190A RhoGAP Ab (Upstate). The amounts of phosphorylated p190A RhoGAP were determined by immunoblot analysis with anti-p190A RhoGAP-pS1150 Ab. The amounts of phosphorylated and total MYPT1 were examined as a positive control. *B*, effect of Rho-kinase-specific inhibitor on ET-1-induced sustained RhoA activation. After serum depletion for 8 h, the cells were incubated with 20 μM Y-27632 or DMSO for 30 min, and then stimulated with 1 μM ET-1 for the indicated periods of time. The cells were lysed with lysis buffer, and the lysates were incubated with GST-Rhotekin-RBD to precipitate the GTP-bound active form of RhoA. The eluates were analyzed by immunoblotting with anti-RhoA Ab. *C*, ET-1-induced sustained phosphorylation of p190A RhoGAP in cultured vascular smooth muscle cells. The cells were transiently transfected with GFP-p190A RhoGAP-FL with the use of the Nucleofector system. After serum depletion for 8 h, the cells were incubated with 20 μM Y-27632 or DMSO for 30 min, and then stimulated with 1 μM ET-1 for the indicated periods of time. The cell lysates were subjected to SDS-PAGE followed by immunoblot analysis with anti-p190A RhoGAP-pS1150 Ab, anti-p190A RhoGAP Ab (Pharmingen), anti-MYPT1-pT853 Ab, and anti-MYPT1 Ab. *D*, effect of ET-1 antagonists on RhoA activity. The cells were starved for serum of 8 h and then stimulated with 1 μM ET-1 for 3 min after treatment with 1 μM BQ-123 or 1 μM BQ-788 for 30 min. The cells were lysed with lysis buffer, and the lysates were incubated with GST-Rhotekin-RBD to precipitate the GTP-bound active form of RhoA. The eluates were analyzed by immunoblotting with anti-RhoA Ab (*top*). The ratio of GTP-RhoA to total RhoA is shown (*bottom*). *E*, effect of ET antagonists on phosphorylation of p190A RhoGAP. The cells were transiently transfected with GFP-p190A RhoGAP-FL. Twenty-four hours after transfection, the cells were starved for serum of 8 h and then stimulated with 1 μM ET-1 for 3 min after treatment with BQ-123 (1 μM, 0.1 μM) or BQ-788 (1 μM, 0.1 μM) for 30 min. The cell lysates were subjected to immunoblot analysis with anti-p190A RhoGAP-pS1150 Ab and anti-p190A RhoGAP Ab (Pharmingen). These results are representative of three independent experiments.